T.C.
ERZİNCAN BİNALİ YILDIRIM UNIVERSITY
INSTITUTE OF NATURAL AND APPLIED SCIENCES

MSc THESIS

SYNTHESIS AND CHARACTERIZATION OF TiO_2 NANOTUBES COATED WITH Cu_2SnS_3 VIA SPRAY PYROLYSIS METHOD FOR ENHANCED PHOTOCATALYTIC ACTIVITY

Abdlrahem ALWAJEDI

Supervisor: Prof. Dr. Çağrı ÇIRAK

PHYSICS
DEPARTMENT

ERZİNCAN
2022

ABSTRACT

MSc Thesis

SYNTHESIS AND CHARACTERIZATION OF TiO_2 NANOTUBES COATED WITH Cu_2SnS_3 VIA SPRAY PYROLYSIS METHOD FOR ENHANCED PHOTOCATALYTIC ACTIVITY

Abdlrahem ALWAJEDİ

Erzincan Binali Yıldırım University
Graduate School of Natural and Applied Sciences
Department of Physics

Supervisor: Prof. Dr. Çağrı ÇIRAK

Much effort is expended in developing improved physicochemical methods for removing dangerous chemical compositions from the air, soil, and water. This present research describes the production of Cu_2SnS_3_TiO_2 nanotubes (CTS_TNT) nanocomposite films for prospective use as photocatalysts in the heterogeneous photodegradation of Rhodamine B under UVA irradiation and visible light. Cu_2SnS_3 coated TiO_2 nanotubes were effectively produced in a two-step process. First, anodic oxidation was used to grow TiO_2 nanotube. After that, Cu_2SnS_3 layer-shaped nanostructures were relatively filled and coated on the top of tubes via spray pyrolysis method in different coating times 3, 5 and 7 minutes. CTS_TNT were characterized by using FESEM and XRD. The characterization results showed that the crystal structure, morphology, elemental composition and density of Cu_2SnS_3 nanolayer on the surface of TiO_2 nanotubes are affected by Cu_2SnS_3 coating time. The photodegradation results demonstrated that the photocatalytic activity of CTS_TNT films increased gradually with increasing Cu_2SnS_3 coating duration. The best performance was achieved in CTS coated sample for 5 minutes. RhB photodegradation efficiency was determined to be 65% for bare TiO_2 and 98 % for (CTS_TNT_5 minutes) coated film under a UV source. Also, photocatalytic performance of TiO_2 nanotubes was enhanced under visible light irradiation by CTS decoration.

2022, 55 Pages

Keywords: Anodic oxidation, CTS, Photocatalytic activity, Rhodamine B, Spray pyrolysis, TiO_2 nanotubes

ÖZET

Yüksek Lisans Tezi

ARTIRILMIŞ FOTOKATALİTİK AKTİVİTEYE SAHİP Cu_2SnS_3 İLE KAPLANMIŞ TiO_2 NANOTÜPLERİNİN SPREY PİROLİZ YÖNTEMİ İLE SENTEZİ VE KARAKTERİZASYONU

Abdlrahem AL WAJEDI

Erzincan Binali Yıldırım Üniversitesi
Fen Bilimleri Enstitüsü
Fizik Anabilim Dalı

Danışman: Prof. Dr. Çağrı ÇIRAK

Havadan, topraktan ve sudan tehlikeli kimyasal bileşimleri uzaklaştırmak için gelişmiş fizikokimyasal yöntemler oluşturmak için birçok çalışma yapılmaktadır. Bu araştırma, UVA ışıması ve görünür ışık altında RhB 'nin heterojen fotodegradasyonunda fotokatalizör olarak prospektif kullanım için Cu_2SnS_3/TiO_2 nanotüplerin (CTS_TNT) nanokompozit filmlerinin üretimini açıklamaktadır. Cu_2SnS_3 kaplı TiO_2 nanotüpler, iki aşamalı bir işlemde etkili bir şekilde üretildi. İlk olarak, TiO_2 nanotüp dizilerini büyütmek için anodik oksidasyon yöntemi kullanıldı. Daha sonra Cu_2SnS_3 tabaka şeklindeki nanoyapılar, 3, 5 ve 7 dakikalık farklı kaplama sürelerinde sprey piroliz yöntemi ile tüplerin üst kısımlarına nispeten doldurulmuş ve kaplanmıştır. (CTS_TNT), FESEM, XRD kullanılarak karakterize edildi. Karakterizasyon sonuçları, TiO_2 nanotüplerin yüzeyindeki Cu_2SnS_3 nanotabakanın kristal yapısının, morfolojisinin, elementel bileşiminin ve yoğunluğunun Cu_2SnS_3 kaplama süresinden etkilendiğini göstermiştir. Fotodegradasyon sonuçları, CTS_TNT filmlerinin fotokatalitik aktivitesinin artan Cu_2SnS_3 kaplama süresi ile kademeli olarak arttığını ve en iyi performansın 5 dakika boyunca kaplanan film için gözlemlendiğini göstermiştir. UV kaynağı altında TNT için %65 ve (CTS_TNT_5 dakika) kaplı film için %98 RhB fotodegradasyon verimi belirlendi.

2022, 55 Sayfa

Anahtar Kelimeler: Anodik oksidasyon, CTS, Fotokatalitik aktivite, Rodamin B, Sprey piroliz, TiO_2 nanotüpler

ACKNOWLEDGEMENT

I would like to express my deep and sincere gratitude to my research supervisor, Prof. Dr. Çağrı ÇIRAK for allowing me to do research and providing invaluable guidance throughout this research. His dynamism, vision, sincerity and motivation have deeply inspired me. I would also like to thank him for his friendship.

I am also grateful to my friends and laboratory colleagues, for their editing help, late-night feedback sessions, moral support and their constant encouragement. It was a great honor to work with you.

I would be remiss in not mentioning my family, their belief in me has kept my spirits and motivation high during this process and for all the emotional support.

Finally, my thanks go to all the people who have supported me to complete the research work directly or indirectly.

Abdlrahem ALWAJEDI
September, 2022

CONTENTS

Page

ABSTRACT ..... **i**
ÖZET ..... **ii**
ACKNOWLEDGEMENT ..... **iii**
CONTENTS ..... **iv**
LIST OF FIGURES ..... **vi**
LIST OF TABLES ..... **viii**
SYMBOLS AND ABBREVIATIONS ..... **ix**
1. INTRODUCTION **1**
.2 **LITERATURE SURVEY** **3**
3. BASICS **8**
3.1. Semiconductors 8
3.1.1. P-type semiconductor 10
3.1.2. N-type semiconductors 10
3.2. TiO_2 Properties 11
3.3. Cu_2SnS_3 (CTS) Properties 14
3.4. Thin Film Technologies 17
3.5. Thin Film Production Techniques 17
3.5.1. Physical deposition techniques 19
3.5.2. Chemical deposition techniques 21
3.5.2.1. Hydrothermal method 21
3.5.2.2. Spray pyrolysis 22
3.5.2.3. Anodic oxidation 23
3.6. Formation Mechanism of TiO_2 Nanotubes 24
3.7. Photocatalysis 26
3.7.1. Photocatalytic degradation mechanism on TiO_2 27
4. MATERIALS AND METHODS **29**
4.1. Preparation of The TiO_2 Nanotube Samples 30
4.2. Preparation of CTS_TNT Composite By Using Spray Pyrolysis Method 33
4.3. CTS_TNT Photocatalytic Performance Tests 35
4.4. Characterization 36
4.4.1. XRD (X-ray diffraction) 36

4.4.2. Scanning electron microscope (SEM) and Energy dispersive X-ray spectroscopy (EDX). 37
5. RESULTS AND DISCUSSION 38
5.1. Cu_2SnS_3 Nanolayer / TiO_2 Nanotubes Nanocomposite Characterization 38
5.1.1. Morphological characterization 38
5.1.2. Crystallographic characterization 40
5.2. Photocatalytic Degradation Tests 41
5.3. Structural Analysis 44
5.4. Degradation Kinetic of RhB on CTS_TNT 45
6. CONCLUSION 47
REFERENCES 48

LIST OF FIGURES

Page

Figure 3.1. Energy levels of conductor, semiconductor and insulator atoms. 9
Figure 3. 2. P-type semiconductors 10
Figure 3. 3. N-type semiconductors 11
Figure 3. 4. Shows the three different crystalline phase of titanium dioxide 13
Figure 3.5. Crystal structures of CTS 16
Figure 3. 6. Applications of thin film technology. 18
Figure 3.7. The techniques of thin films 20
Figure 3.8. Hydrothermal system 21
Figure 3.9. Spray pyrolysis system 22
Figure 3.10. Anodic oxidation 23
Figure 3.11. TNT's process of creation 25
Figure 3.12. Shown schematically the Nanopore growth vs current-time transient. 25
Figure 3.13. Schematic of TiO_2 photocatalytic mechanism. 28
Figure 4.1. Production process of CTS/TNT films 29
Figure 4.2. Ultrasonic bath that used in cleaning process 30
Figure 4.3. Magnetic stirrer 31
Figure 4.4. Anodization setup 31
Figure 4.5. Formation mechanism of TiO_2 nanotube arrays. 32
Figure 4.6. Used furnace for annealing the TNT 32
Figure 4.7. Time variation of temperature during annealing of TNT 33
Figure 4.8. The mixture device 33
Figure 4. 9. Air pressure control device 34
Figure 4.10. The system of spray pyrolysis coating 34
Figure 4.11. UV source 35
Figure 4.12. Solar simulator, visible light 35
Figure 4.13. UV-Vis spectrophotometer 36
Figure 4.14. X-Ray diffraction device 36
Figure 4.15. Field Emission Scanning Electron Microscopy (FESEM) 37
Figure 5.1. Bare TNT 38
Figure 5.2. CTS_TNT_3 minutes 38

Figure5.3.CTS_TNT_5minutes……...39
Figure 5.4. CTS_TNT_7 minutes 39
Figure 5. 5. Cross section of CTS_TNT_7 minutes.....39
Figure 5.6. XRD patterns of TNT bare, (CTS_TNT_3 min), (CTS_TNT_5 min) and (CTS_TNT_7 min). A: anatase and T: titanium. 40
Figure 5.7. Photodegradation of RhB under UV light by bare TNT, (CTS_TNT 3min), (CTS_TNT_5 min) and (CTS_TNT_7 min) films.....41
Figure 5.8. The degradation of RhB under visible light by bare TNT (CTS_TNT 3min), (CTS_TNT_5 min) and (CTS_TNT_7min) films.....42
Figure 5.9. Comparison of photodegradation performance percentage under visible and UV light.....43
Figure 5.10. Photostability tests of (CTS_TNT_5min) by photodegradation of RhB under UV light. 43
Figure 5.11. EDX spectra of (CTS_TNT_5 min) film.....44
Figure 5.12. RhB degradation reaction kinetics fit under visible light. 46
Figure 5. 13. RhB degradation reaction kinetics fit under UV light. 46

LIST OF TABLES

Page

Table 3.1. Some properties of three main phases of TiO_2 14
Table 3.2. shows the various CTS structures. 16
Table 5.1. Percentage of presence of elements by EDX. 44
Table 5.2. Apparent pseudo first-order rate constants (kapp), and correlation coefficients (R-square). 45

SYMBOLS AND ABBREVIATIONS

Symbols

%	Percent
~	Approximately
C	Celsius degree
cm	Centimeter
Ev	Electron volt
g	Gram
I	Intensity
L	Liter
M	Mol
Nm	nanometer
NP	Nano particle
PH	Potential of hydrogen
R^2	Interaction rate
TNT	Titanium nano tubes
W	Watt
μm	Micrometer
Ω	Ohm

Abbreviations

AFM	Atomic force microscopy
CB	Conduction band
CdS	Cadmium sulfide
CTS_TNT	Cu_2SnS_3 nanolayer _ TiO_2 Titanium nano tubes
Cu	Copper
CVD	Chemical vapor deposition
DSSC	Dye sensitive solar cell
EDX	Energy dispersive X-ray analysis
EG	Energy band gap
Fe_2O_3	Ferric Oxide
FESEM	Field emission scanning electron microscopy
FTIR	Fourier transform infrared spectroscopy

MB	Methylene blue
MO	Methyl orange
NH_4F	Ammonium fluoride
PVD	Physical vapor deposition
RhB	Rhodamine B
S	Sulphur
Sn	Tin
TEM	Transmission electron microscope
TiO_2	Titanium dioxide
TNT	Titanium nano tubes
UV	Ultra violet
UV-DRS	UV-vis reflectance spectroscopy
VB	Valance band
XPS	X-ray photoelectron spectroscopy
XRD	X-ray diffraction
ZnO	Zinc dioxide

1. INTRODUCTION

Wastewaters from various industries, factories, labs, and other sources have become a severe environmental issue. Dye-containing wastes released into the environment are harmful to microorganisms, aquatic life, and humans. A lot of work is performed to create enhanced physicochemical methods for removing dangerous chemical Toxic substances and pollutants from water. Due to their mineralization capability and potential application to water pollution control using solar energy, which is a renewable energy source, cost-effective, and entirely free to degrade organic compounds by photolysis, semiconductor photocatalysts have received special attention in organic compound degradation (Borker and Salker, 2006).

Semiconductors such as (TiO_2, ZnO, Fe_2O_3, CdS, and ZnS) have the potential to function as catalysts for oxidation and reduction processes. Semiconductors structure is characterized by a complete valence band and an empty conduction band. Among all of these semiconductor catalysts, titanium dioxide (TiO_2) is the most widely used semiconductor catalyst in photoinduced processes because it is chemically and biologically inactive, staple photocatalytic, relatively easy to produce and use, capable of efficiently catalyzing reactions, inexpensive, and poses no dangers to the environment or humans (Akpan and Hameed, 2009).

Especially anodic TiO_2 nanotubes have piqued the interest of many researchers because they provide a great level of control over the separation of photogenerated charge carriers, not only in photocatalytic but also in photoelectrochemical processes (Zhou, Liu and Schmuki, 2017). However, when exposed to visible light or sunlight, the nanostructured TiO_2 materials' catalytic activity is severely hindered because of the huge band gap and rapid electron-hole recombination, as a consequence of this limitation, Several investigations and research projects have been carried out to overcome it and boost the activity of degradation of TiO_2 nanoparticles on toxic organic and chemical degradation. In these research, both doping the TiO_2 lattice with metallic or non-metallic atoms and providing inert support have been included. Despite this, the findings of these investigations are still inadequate (Schneider *et al.*, 2014; Qiu *et al.*, 2015).

Using composite semiconductors, the photocatalytic activity can be improved by enhancing the charge transfer and extending the energy range of photo-excitation. Composite semiconductors photocatalysts display extremely photocatalytic activity for liquid-phase processes. Researchers have been interested in pairing two semiconductor particles with different band-gap widths for some years, and several research groups have conducted photocatalytic activity investigations on various composited semiconductor particle systems, such as TiO_2/SnO_2 (Vinodgopal and Kamat, 1995), TiO_2/WO_3 (Li *et al.*, 2001), TiO_2/MoO_3 (Song *et al.*, 2001), TiO_2/CdS (Vogel, Hoyer and Weller, 2002), TiO_2/ZrO_2 (Yu, Lin and Kwok, 1998) and TiO_2–Fe_2O_3 (Pal *et al.*, 2001). However, the photocatalytic activity of nanocomposite TiO_2/Cu_2SnS_3 is little reported.

As far as we know, creating a Cu_2SnS_3 nanolayer on TiO_2 nanotubes nanocomposite by spray pyrolysis method has not yet been reported for photocatalytic activity.

Furthermore, no extensive research has been undertaken to illustrate the influence of Cu_2SnS_3 on the structural and morphological characteristics of TiO_2 nanotubes / Cu_2SnS_3 nanolayer nanocomposites (CTS_TNT).

In this work, an easy-to-make approach for producing TiO_2 nanotube / Cu_2SnS_3 nanolayer nanocomposites by anodic oxidation and spray pyrolysis method is given. CTS/TNT films have been characterized by field emission scanning electron microscopy (FESEM) and X-ray diffraction (XRD).

The influence of Cu_2SnS_3 coating duration on the performance of photocatalysis activity was also examined by a UV-vis spectrometer.

2. LITERATURE SURVEY

Iijima is considered the first to invent carbon nanotubes, which have engineering properties that not only contributed to the development of the technological field, but also the field of physics, chemistry and biology (Iijima, 1991).

The majority of inorganic nanotubes are created to take use of other material-specific features, and the primary areas of interest for their use are in the fields of biomedicine, photochemistry, electricity, and the environment (Roy, Berger and Schmuki, 2011).

Zwilling and his colleagues reported the earliest examples of self-organized anodic oxides on titanium for anodization in chromic acid electrolytes, which also included hydrofluoric acid. The tube structure was not very well ordered, and the sidewalls of the tubes had a significant amount of inhomogeneity (Zwilling *et al.*, 1999).

However, it was found that making just small additions of fluoride ions to an electrolyte was what was necessary to bring about the formation of these self-organized oxide structures (Berger and Schmuki, 2011).

Kelly examined how the presence of fluoride ions affects the process of passive dissolution of titanium. Using steady state potential step, and impedance measurements, an investigation of the effect that fluoride ions have on the passive dissolution of titanium in a 4.5 M H_2SO_4 solution was carried out. Metal dissolution happens via a surface coating, which was validated by an Sem examination. This material was identified as polycrystalline TiO_2 by electron diffraction and SIMS studies. A mechanism that involves the production and breakdown of surface oxide at the same time has been presented as a possible explanation for the observations. The field exerts an influence on the ionic current that is moving through the film. The amount of fluoride present in the solution is the primary factor that determines how quickly the oxide will dissolve (Kelly, 1979).

Fang, titanium electrodes underwent an electrolytic anodization process, which resulted in the formation of TiO_2 nanotubes highly ordered in their study to assess the influence of heat treatment on the morphology, crystal structure, and photocatalytic of TiO_2 nanotubes' characteristics when grown on titanium substrates, and independent

membrane. (SEM),(TEM), and X-ray diffraction were used to study the morphological evolution and phase changes of TiO_2 nanotubes on a Ti substrate in addition to separate TiO_2 membranes throughout the calcination process (XRD). They discovered that at 600 °C, there was a composite layer placed between the tube layer and the titanium substrate, and as a consequence of their investigation, the length of the nanotubes was significantly reduced when heated to 750 degrees Celsius. They also tested the catalytic activity of TiO_2 nanotubes on a titanium substrate that had been annealed at different temperatures by dissolving methyl orange in an aqueous solution while being exposed to UV light. As a consequence, they discovered that TiO_2 nanotubes annealed at 450 °C with pure anatase crystals exhibit greater catalytic activity than any of those annealed at 600 °C or 750 °C. This occurred because anatase crystals were present in the tube layer of the TiO2 nanotubes, whereas rutile crystals were present in the compact layer of the nanotubes (Fang *et al.*, 2011).

Kustiningsih investigated photocatalytic Degradation of Organic Waste in Visible light using TiO_2 Nanotubes Array investigated, The use of a TiO_2 nanotubes array to photocatalyze the breakdown of organic waste has been examined. In this study, phenol was employed as an organic waste. Titania nanotubes were produced using anodization at a voltage of 50 V for two hours with the electrolyte solution consisting of 98% ethylene glycol and 0.5% wt Nh_4F. Analyses of the manufactured catalysts were carried out using a variety of techniques, including (SEM), X-ray diffraction (XRD), Fourier transform infrared spectroscopy (FTIR), and UV-vis reflectance spectroscopy (UV-DRS). The impact of pH and phenol content at the start has been studied. The results revealed that pH 5 was the optimal pH for phenol decomposition. For 180 minutes, the phenol concentration was lowered from 40 ppm to 6.9 ppm under this setting (Kustiningsih *et al.*, 2020).

Peral and his colleagues have described how photocatalysis may be used to purify, decontaminate, and deodorize air. Mills and his colleagues investigated semiconductor-sensitized photosynthesis and photocatalytic processes for the removal of organic compounds, the destruction of cancer cells, and the elimination of bacteria and viruses (Pangarkar and Beenackers, 2002).

Rahaman and his colleagues researched to investigate the impact of copper concentration on CTS thin films for use in photocatalysis applications and solar cell absorber layers. The effect of Copper Concentration on the Electrical, Optical, and

Structural Properties of CTS Thin Films, they claim in their study. The production of a tetragonal structure in CTS films with orientation along the (112) plane is confirmed by XRD and TEM data. In films with greater Cu concentrations, Raman research supports the tetragonal geometry of the Cu_2SnS_3 film and the Cu_2S secondary phase. For 0.025M Cu concentration, a stoichiometric film is discovered. XPS and PL experiments are also carried out. CTS films have an absorbance coefficient of ~10^5 cm^{-1} and a bandgap ranging from 1.32 eV to 1.49 eV. Electrical properties with a carrier concentration of ~$10^{21}/cm^3$ reveal the film's P-type semiconductor nature. As the Cu content increases, the film's resistivity reduces from 4.6 x 10^{-1} to 9.5 x 10^{-4} Ω-cm. These characteristics are ideal for the absorber layer of a solar cell. The photocatalytic performance of methylene blue (MB) dye is investigated using the optimized CTS film as a photocatalyst exposed to irradiation of visible light. Under 3 hours of visible light irradiation, MB photodegraded significantly by (~90%) (Rahaman *et al.*, 2020).

Van Viet and his team performed investigations. It has been determined that the temperature at which annealing is performed affects the crystalline structure, shape, and photocatalytic activity of Ag-TiO_2 nanotubes. According to their observations, the structure of the TNT started to fracture at high annealing temperatures (more than 400 °C), and it completely fell apart at 500 °C. The researchers found that Ag_TNTs that were annealed at 300 °C had a strong capacity to photodegrade MB for 150 minutes when exposed to sunlight. They also found that the average diameter of Ag NPs in Ag/TNTs rose linearly with the annealing temperature (Van Viet *et al.*, 2018).

Çırak and his teamwork investigated the production of WO_3 coated TiO_2 nanotube array electrodes and found that they had improved photoelectrochemical performance for the degradation of rhodamine B dye Preparation, characterization, and superior photoelectrochemical performance. By electrochemically depositing WO_3 on a titanium nanotube (TNT) array and cycling the voltage between -0.6 and 1.0 V against Ag/AgCl, an effective photoelectrocatalyst was created in their work. X-ray photoelectron spectroscopy (XPS), X-ray diffraction (XRD), and scanning electron microscopic (SEM) techniques were used to characterize the Electrode structure and morphology (TNT-Wo_3), additionally, WO_3 species successfully decorated TNT surfaces, and this was done without the creation of any other oxidation species. Then, under UV light irradiation, the photoelectrocatalytic activity of the composite electrode operating at 0.2 V (Ag/AgCl) was examined using model pollutants Methylene blue (MB), Orange G

(OG), and Rhodamine B (RhB). The electrode has delivered the greatest performance against RhB among the azo dyes examined (Çırak, B. B *et al.*, 2021).

Çırak and his colleagues studied the Synthesis and characterization of ZnO nano-rice decorated TiO_2 nanotubes for enhanced photocatalytic activity, To employ as photocatalysts in the heterogeneous degradation of Rhodamine B when exposed to UV light, they reported the production of TiO_2/ZnO nanocomposite (TZN) films. A simple and practical two-step method for making ZnO-coated TiO_2 nanotubes was developed. Anodic oxidation was first used to create TiO_2 nanotube arrays. Following that, the CBD method was used to coat nanotubes with ZnO rice-shaped nanostructures by 2, 4, 6, and 8. The photocatalytic performance steadily rose with the rise in the number of deposition cycles. The best possible efficiency was achieved using the 8-cycle sample. The photodegradation efficiency of RhB was found to be 65 percent for bare TiO_2, but 95 percent for the 8-cycle coated sample. In addition, all the samples exhibited high reusability and photostability by checking their performance four times. The photocatalytic performance of the samples was examined by UVC, UVB, UVA, and visible irradiation for comparison purpose (Çırak *et al.*, 2019).

In their research, Zarepour and Tasviri looked into the synthesis and characterisation of ZnO nano-rice coated TiO_2 nanotubes for increased photocatalytic activity. In the present article, solvothermal TiO_2 nano-rice was produced, and the influence of silver nanoparticle impact of deposition on the behavior of photocatalysis of generated TiO_2 was thoroughly examined. The major phase of produced TiO_2 is Rutile, according to the XRD pattern. The nano-rice structure of TiO_2 was shown by SEM pictures and EDX analyses, as well as the presence of silver nanoparticles. As usual, the analysis equipment was used to analyze the surface of the samples and check their nano structure. According to TEM pictures On the top surface of the TiO_2 nano-rice, the AgNPs are scattered uniformly in a random pattern. The photocatalysis of the produced samples containing varying quantities of Ag molecules was examined in depth. The activity status of photocatalytic of The best pollution model materials was TiO_2 with 0.125 % Ag to degrade Acid Blue 92 and Crystal Violet. After 90 minutes, Acid Blue 92 and Crystal Violet deterioration using this photocatalyst is 72 % and with 0.0139 min^{-1} and 0.008 min^{-1} the photocatalysis is 53.16 % rate constants. According to the reusability tests and TEM, analyzation synthesized samples demonstrated high stability (Zarepour and Tasviri, 2019).

Hong Lai and Hamid produced WO_3 nanoparticles covered with TiO_2 nanotube hybrid material for efficient photocatalytic behavior. Moreover, in this particular piece of research, nanotubes were characterized utilizing FESEM, EDX, XRD, and Raman spectroscopy. The pore measure of nanotubes is the width of up to 74 nm and a length of 1.6 µm was created based on the findings. By using EDX T tungsten existing in the nanotube arrays was demonstrated, with tungsten concentration ranging from 1.06 % percent to 3.29 %. After that, The nanotube arrays' photocatalytic behavior was then investigated utilizing methyl orange degradation under TUV 96W UV-B light. Tungsten was found to have the greatest photocatalytic activity because of the large number of photo-induced electron-hole pairs that it formed and its existence (Hong, Lai and Hamid, 2015).

3. BASICS

3.1. Semiconductors

Semiconductors are becoming increasingly significant in today's society. The functions of oxide semiconductors have been widely investigated, with industrial applications such as thin film transistors and transparent electrodes emerging in recent decades (Oba and Kumagai, 2018).

Solids are classified as conductors, semiconductors, and insulators based on their electronic behavior, which is measured by the energy band gap (Eg). Band theory, which is based on the molecular orbital (MO) theory, can explain the distinctions between conductors, semiconductors, and insulators. Electrons can travel from the valence band which is full of electrons, in addition as the highest occupied molecular orbital, the highest occupied molecular orbital corresponds to the empty conduction band, Likewise referred to as the lowest empty molecular orbital, when they receive enough energy.

Conductors are typically metals or alloys with a lot of free electrons in the valence band. Because of the absence of an intervening gap between both the valence and conduction bands of a conductor, electrons are transported easily from the valence to the conduction bands in a conductor material even when just a little amount of energy is provided. Conductors include copper (Cu), silver (Ag), and aluminum (Al).

Insulators, which are nonmetals, Even though huge quantities of energy are provided, electrons may not migrate because the band gap between the conduction and valence bands is too wide. Insulators come in three varieties: solid, liquid, and gas.

In a semiconductor called metalloids, Between the valence and the conduction band, there is a tiny energy band gap bigger than the conductor's band gap and smaller than the insulator's band gap, thus electrons are transported when enough energy is applied. Semiconductors have a lower conductivity than insulators but a higher conductivity than conductors. Furthermore, semiconductors have a tough and brittle structure with a negative temperature resistance coefficient (NTC) (Gupta and Gupta, 2016). As shown in Figure 3.1 the energy band gap structure of conductors, insulators and

semiconductors. The most electrons occupied band is known as the valence band, while the Slightly filled with electrons band is known as the conduction band.

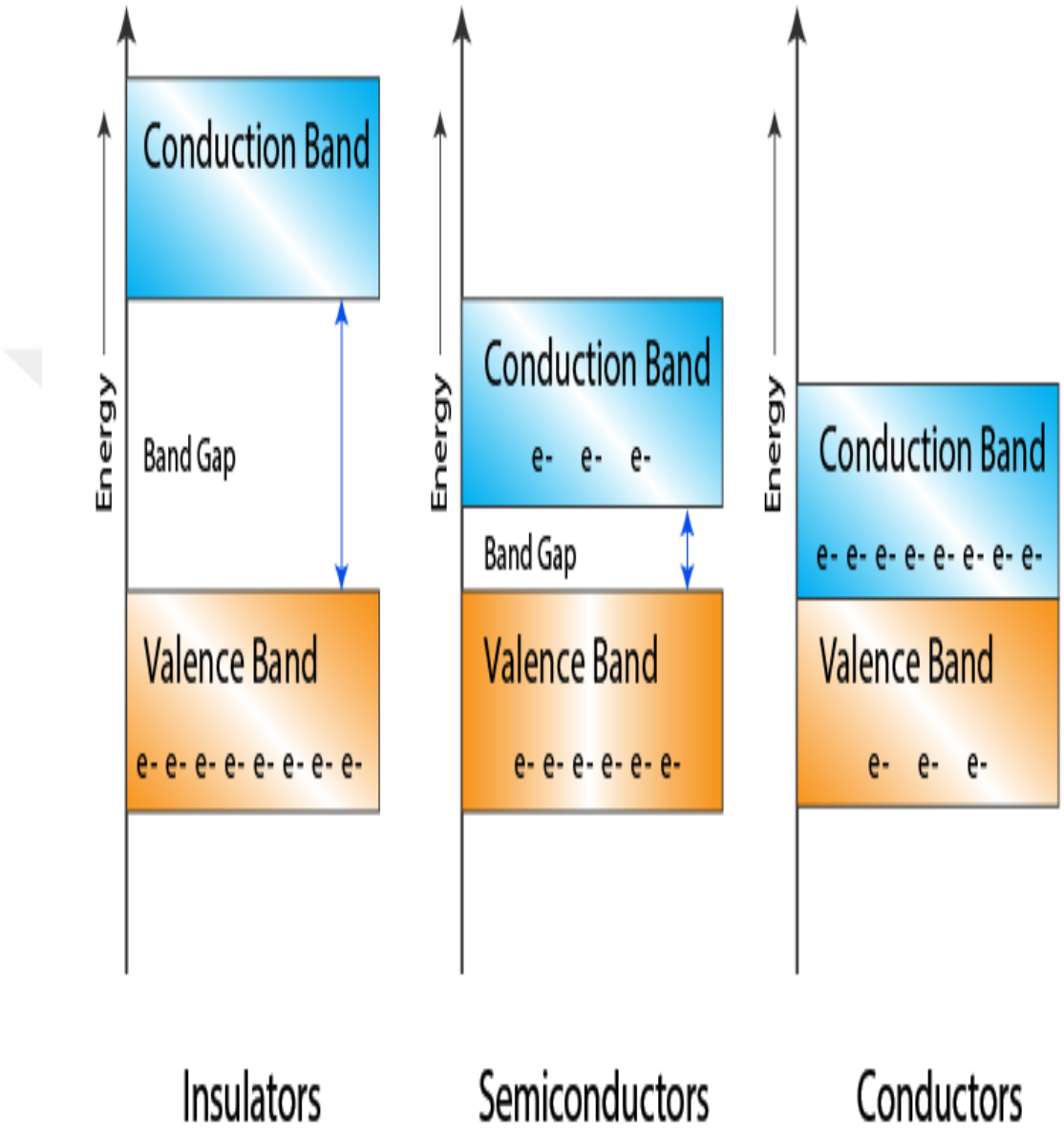

Figure 3.1. Energy levels of conductor, semiconductor and insulator atoms (Bıyıklı, 2020).

Semiconductors are split and categorized into two types: n-type and p-type. Current in a semiconductor is carried by the mobility of electrons and holes that can roam freely (charge carriers). The generated rate of charge carriers can be raised through a form of

modification procedure known as doping, which involves adding impurity to the structure of the substance (Onay, 2021).

3.1.1. P-type semiconductor

It is formed by mixing group elements such as germanium or silicon from the periodic table. That elements containing three electrons in the valence orbit, Indium (In), gallium (Ga), and boron are examples of these elements (B). When germanium or silicon, which has four electrons in its orbital, is mixed with indium, which has three electrons in its last orbital, three electrons form covalent connections with nearby electrons. When one of the silicon or germanium electrons cannot find another electron to attach to, a hole emerges that requires electrons as shown in Figure 3.2. Vacancies are regarded positively charged. These gap-rich mixtures are known as P-type semiconductors (Beşli, 2012; Eden, 2019).

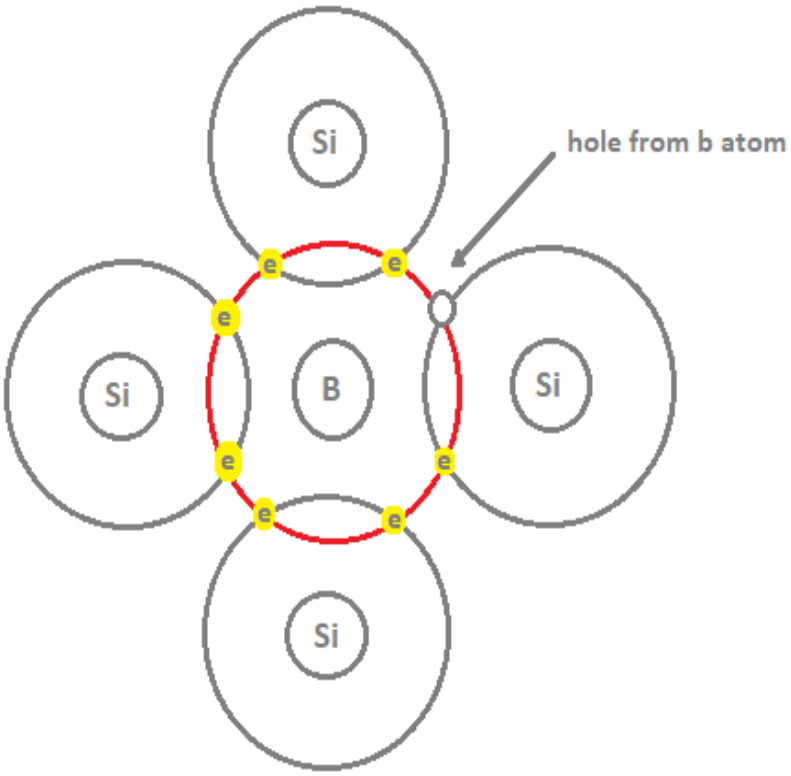

Figure 3.2. P-type semiconductors

3.1.2. N-type semiconductors

When a semiconductor material is doped, it becomes an n-type semiconductor, showing an increase in the amount of negatively charged electrons in the conduction band. The

periodic table's germanium and silicon are N-type semiconductors. It is created by combining the group's elements (with 5 electrons in their valence orbital). Arsenic, antimony, and phosphorus are examples of these elements. When 4 electrons in the last orbit of germanium or silicon are combined with 5 electrons in the last orbit of phosphorus, 4 electrons in the phosphorus establish covalent bonds with nearby electrons as shown in Figure 3.3. In a silicon or germanium crystal, an idle electron circulates freely. N-type semiconductors are made up of electron-rich mixtures (Beşli, 2012; Eden, 2019).

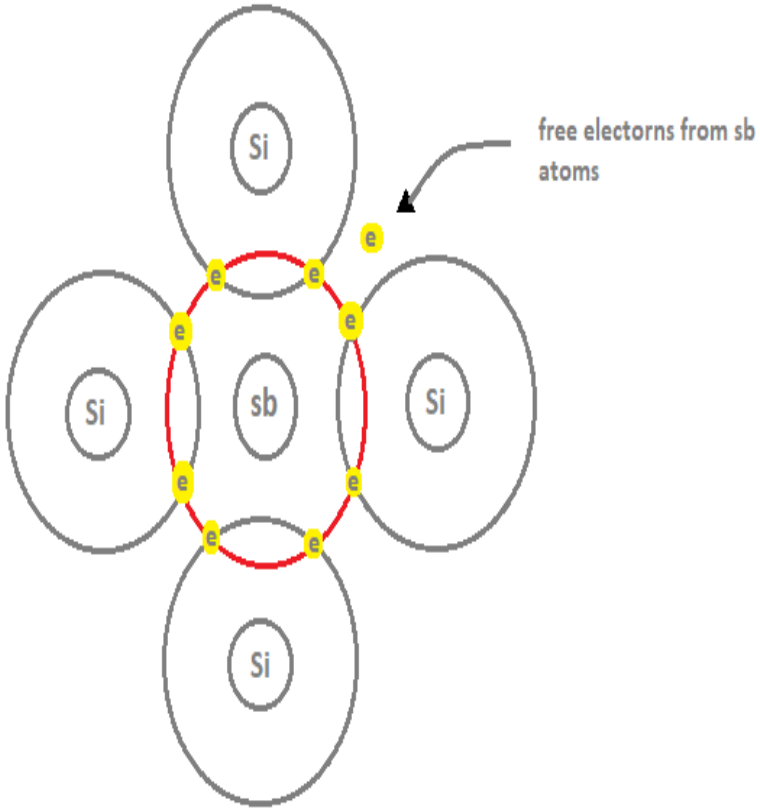

Figure 3.3. N-type semiconductors

3.2. TiO_2 Properties

TiO_2 is currently gaining popularity because of its special physical and chemical properties, which include good photostability, bioactivity, low cost, electron transport and better productivity. TiO_2 nano-materials have been researched for a wide range of applications, including dye-sensitized solar cells, gas sensors, water electrolysis, and pollutant destruction. TiO_2 is the semiconductor that is used the mostly in the production of photocatalysts (Su *et al.*, 2016; Rasoulifard, Fazli and Eskandarian, 2014; Singh *et al.*, 2016). TiO_2 is a chemical element with the symbol IV in the periodic table.

It's a semiconductor substance made out of oxygen, one of the group's elements, bonded together. Anatase, rutile, and brookite are the three types of TiO_2 found in nature which is clearly shown in Figure 3.4. The two most common phases are anatase and rutile. Tetragonal rutile and anatase phases, orthorhombic brookite Anatase and brookite are metastable, whereas rutile is a stable phase in tetragonal structure. The anatase tetragonal and brookite orthorhombic phases were used to crystallize them. Photocatalysts include rutile and anatase phases, with anatase having the greatest photocatalytic action (Çirak and Kavakli, 2016).

Light's involvement as a catalyst in chemical processes is described by the term photocatalysis. In the visible and ultraviolet (UV) spectrums, the wavelength of light required for photocatalysis ranges from 10-7 to 10-6. Titanium dioxide is now being employed as a photocatalyst semiconductor to tackle environmental issues such as water and air cleaning. TiO_2 is a semiconductor with a band gap energy of 3.2 eV. The valence band is constituted of the oxygen 2p orbital, while the conduction band is constituted of the Ti 3d orbital. Electrons in the valence band can be migrated to the conduction band by an external energy source in semiconductors with a wide band gap. During this electron transition, holes develop in the valence band. Semiconductors are unstable in the excited state, while TiO_2 appears to be stable even in the excited state. This property is one of the reasons TiO_2 is such an effective photocatalyst. Semiconductors have a significant impact on photocatalytic processes. In photocatalytic processes involving semiconductors, the band gap energy defines the wavelength of light required for material excitation, and the maximal point of the valence band controls the photocatalyst's oxidation power (Demir, 2018; Baylan, 2011).

The interaction of semiconductor material with light lies at the heart of heterogeneous photocatalysis. The employment of solar light as an energy source for environmental cleansing has given rise to the concept of photocatalysis. The heterogeneous photocatalysis method is a promising and perfect strategy. Titanium dioxide (TiO_2) is the most commonly studied and used photocatalyst among various semiconductors with photocatalytic activity because of its high oxidation potential, low cost, and high efficiency when exposed to ultraviolet (UV) radiation. When TiO_2 is exposed to ultraviolet (UV) light, electron-hole pairs occur. Electron-hole pairs generate (Alduran, 2019).

The most investigated phases for photocatalytic applications are anatase and rutile. Brookite's properties are seldom mentioned since it is difficult to make and is typically considered an inactive photocatalyst, in contrast to the other metastable phases of TiO_2 rutile is the most thermodynamically stable polymorph with a bandgap of 3.0 eV, it is a direct bandgap semiconductor. While, the bandgap of rutile is less than that of other TiO_2 polymorphs, the high rate of generating electrons and holes makes it an unsuitable option for photocatalysis. Above 600°C, anatase TiO_2 becomes metastable, but it is still less stable than rutile. Because it has such low surface energy the anatase phase is the phase that is relatively stable at the nanoscale, making it more efficient for photocatalysis, according to the structured-based analysis. Because anatase has a bandgap of 3.2 eV, its activity threshold is only reached when exposed to UV light,

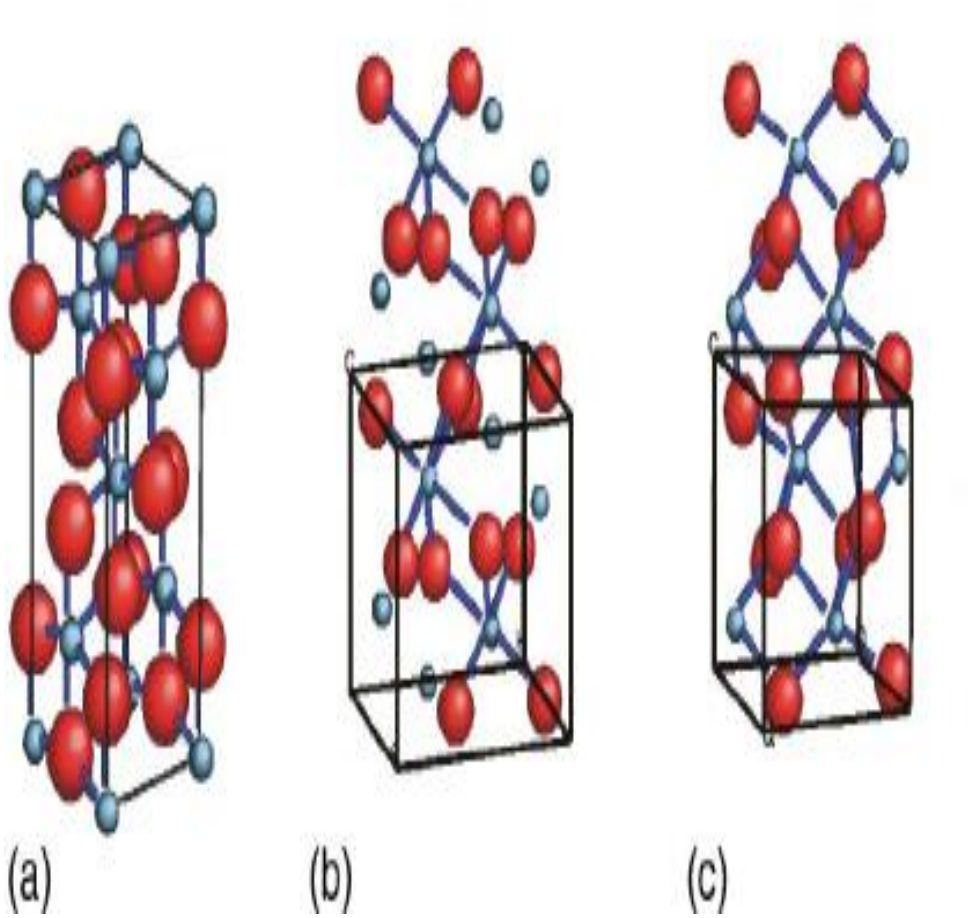

Figure 3.4. Shows the three different crystalline phase of titanium dioxide: (a) anatase, (b) rutile, and (c) brookite (Hearne et al., 2004).

Table 3.1 show some properties of TiO_2 phases. Excited electrons on anatase have sufficient energy to reduce H+ to hydrogen, while holes on anatase have sufficient

energy to oxidize water to oxygen, which aids in the degradation of many organic pollutants. Excited electrons on anatase have an energy level of E = -0.66 eV relative to a standard hydrogen electrode (Ghori, 2018).

Table 3.1. Some properties of three main phases of TiO2 (Zhao et al., 2017; Mo and Ching, 1995)

Property	**Anatase**	**Rutile**	**Brookite**
Crystal structure	tetragonal	tetragonal	orthorhombic
Lattice constants (Å)	a=3.78 c=9.52	a=4.59 c=2.96	a=9.18 b=5.45 c=5.15
Molecule/cell	4	2	8
Band gap (eV)	3.2	3.0	3.2
Density (g/cm3)	3.79	4.13	3.99
Volume/molecule (Å3)	34.06	31.22	32.17

3.3. Cu_2SnS_3 (CTS) Properties

The tripartite Cu–Sn–S system is part of the I–IV–VI group and is made up of elements that are safe to consume, easily accessible, and low-cost. Which are Copper tin and sulfide. Since 1960, researchers have been studying the Cu–Sn–S system due to their acceptable opto-electronic characteristics. Three elements were investigated in this system absorbance material for solar cell and catalytic applications, absorber material

for thin film photovoltaic and attractive raw-material features. Moreover, has gotten a lot of interest as a potential photocatalyst substance for dye breakdown and hydrogen generation in photocatalysis (Yao *et al.*, 2017).

Cu_2SnS_3, Cu_3SnS_4, and Cu_4SnS_4 all of these components had P-type electrical conductivity and direct band gap values ranging from 0.8 to 1.7 eV, with a strong optical absorption coefficient of $\sim 10^5\ cm^{-1}$. Depending on its crystal structure, Cu_2SnS_3 has direct band gaps ranging from 0.93–1.51 eV covering the visible and near-infrared part of the solar spectrum, Table 3.2 shows various CTS structures (Nakashima *et al.*, 2015; Reddy *et al.*, 2019).

TiO_2, ZnS, WO_3, and ZnO, are the most important semiconductor photocatalysts and have been used in a range of environmental processes, including organic pollutant cleanup and electrochemical splitting of water to produce hydrogen and oxygen. However, these materials have huge band gaps as consequence they are only active in the ultraviolet light area for exciting the electrons. To fully utilize solar energy, the band gap must be reduced in order to expand the range of the receptive spectrum beyond UV light and into the visible light that is predominant. These materials, however, are incapable of absorbing visible light, which accounts for about 46% of the total solar energy. Only a few research organizations have investigated novel semiconductor material that has the potential to be utilized in the destruction of environmental contaminants. The fact that the energy band gap of CTS can be tuned makes it a good candidate for photocatalysis driven by visible light. It is desirable to take advantage of low-cost, stable, non-toxic, and new visible light-sensitive semiconductor photocatalysts (Rahaman *et al.*, 2020; Yao *et al.*, 2017).

The CTS compound can be either biomorphic or polymorphic. Cubic, tetragonal, and monoclinic CTS essential phases are the most widely synthesized as shown in Figure 3.5. The creation of phases is determined by the cation organization and the heating rate. The two phases tetragonal and monoclinic are stable at poor temperatures of 750 °C, However, at extreme heat, the cubic form becomes metastable at 4750 °C (Onoda *et al.*, 2000; Hall, Szymanski and Stewart, 1978; Wang, 1974; Lokhande *et al.*, 2016).

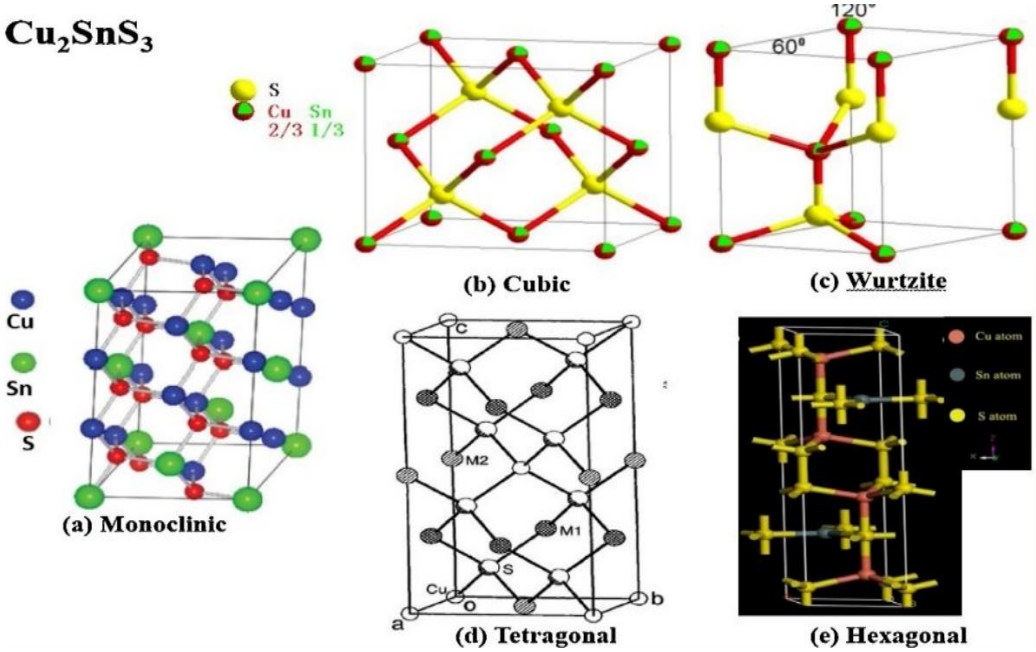

Figure 3.5. Crystal structures of CTS (Reddy et al., 2019).

Table 3.2. shows the various CTS structures, as well as their symmetry and lattice characteristics (Lokhande et al., 2016).

Structure	Symmetry	A (A°)	B (A°)	C (A°)
Monoclinic	*Cc*	6.65	11.54	6.67
Triclinic		6.66	11.48	20.6
Cubic	*F43m*	5.43		
Tetragonal	*F42m*	5.41		10.82
Hexagonal	*P6₃/mmc*	3.90		17.27

3.4. Thin Film Technologies

Thin film technology is one of the earliest arts, dating back to the metal times of antiquity, as well as one of the most recent sciences. The technology of thin films is well understood and has piqued the interest of humans since prehistoric times. More than 2000 years ago, goldsmiths and silversmiths created several procedures for the benefit of all humanity, including the use of mercury (Thirumalai, 2017).

In the role of an adhesive for thin sheets of metal used on sculptures and other things. Ancient mercury-based processes including techniques like silvering and fire gilding were employed to coat less valuable substrates to protect or decorate with tiny layers of gold or silver and it was used for specific purposes (Greene, 2014).

The technology of thin films is one of the most significant approaches that has led to the development of nanotechnology as well as the research of semiconductors and gave a clear idea of many physical properties. Such as physical and engineering qualities, the balance of their micro-structure, the lack of thickness of these membranes and the ease of cracking, so they are deposited on other substances that are utilized as sedimentation bases. Glass, quartz, silicon, aluminum, and titanium are some examples of bases that may be used depending on the nature of the usage and the research (Albashir and Alraheem, 2016).

In addition, thin film applications have evolved significantly over time and have evolved into an essential component of modern-day scientific, industrial, environmental, and medicinal practices. The thicknesses of the films might be between a few tenths of a nanometer and a few micrometers. Thin films are a critical area of study and application. The applications of these thin films shown in Figure 3.6 include, among other things a large and important number of environmental, medical and industrial applications, such as optical, optoelectronic devices, chemistry, gas sensors, electrodynamics, power storage, photo-chemical power conversion, and fuel cells (Stoian *et al.*, 2021).

3.5. Thin Film Production Techniques

Thin film coatings are widely used to prevent surface scratches in electronic devices we use today, as anti-reflective and reflective on glasses and other optical surfaces,

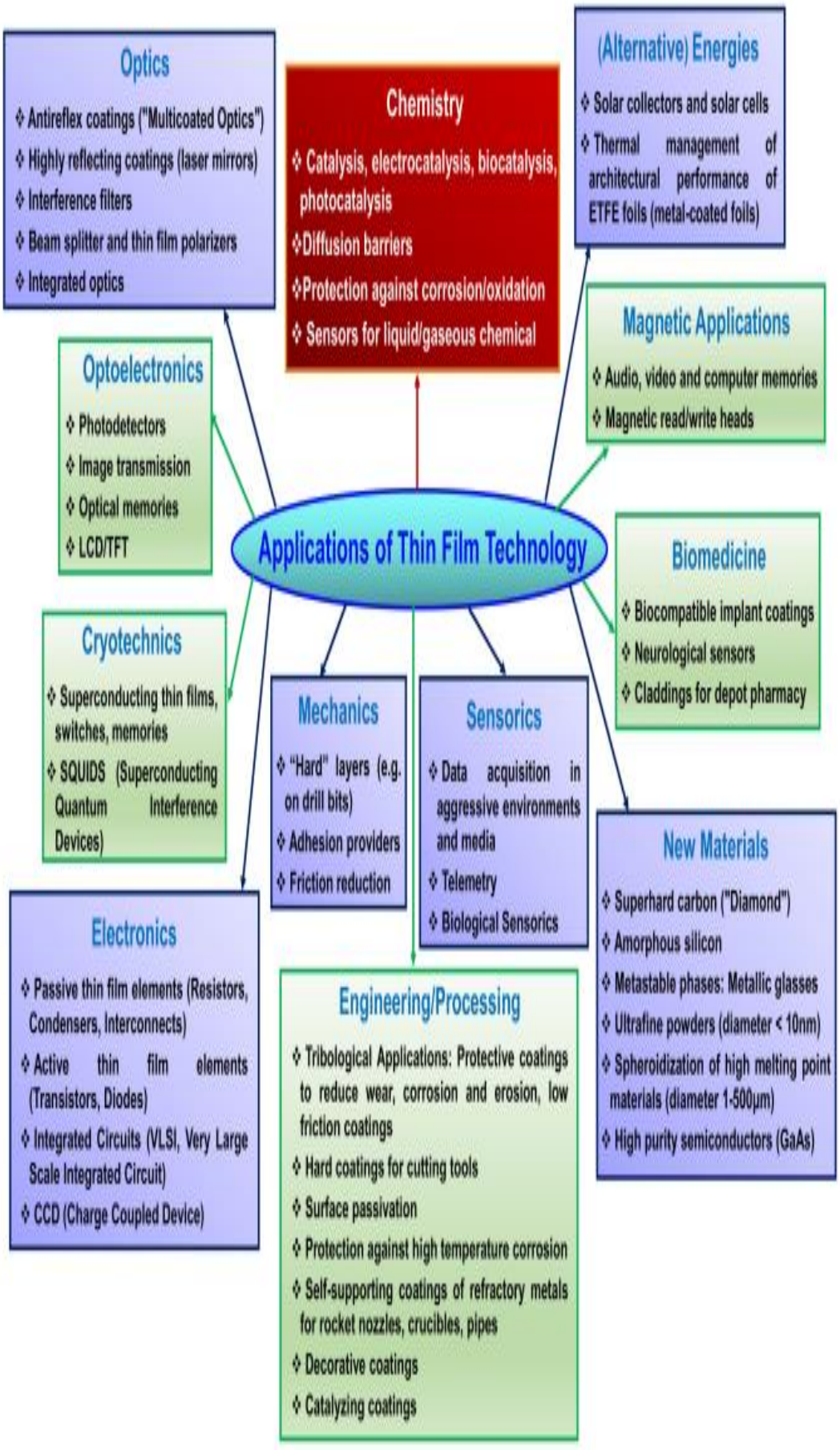

Figure 3.6. Applications of thin film technology (Stoian et al., 2021).

to provide conductivity or insulation in tools and to prevent oxidation. The thin films have a thickness that is lower than 1 micrometer. The process of coating the surface of a material with a very thin layer in order to change or develop the surface Characteristics of a material or to protect the material from external factors is called thin film coating. Thin films, which have a wide range of uses, are used in photovoltaic systems, lenses, sensors, optical filters and many industrial areas. There are many methods to obtain thin films (Sönmezoğlu et al., 2012).

As can be seen in Figure 3.7, the techniques for creating thin films may be divided into two categories: physical methods and chemical methods.

3.5.1. Physical deposition techniques

The physical techniques known as physical vapor deposition (PVD) is used to create thin films by extracting atoms from a solid or liquid using an intense force and then depositing those atoms on a surface that is nearby. Below are some examples of PVD processes (Rossnagel, 2003).

- Sputtering: Sputtering is a well-known PVD technique. In non-thermal vaporization, high-energy ion bombardment causes atomic collision cascades that eject atoms off the target surface (Abegunde *et al.*, 2019; Abegunde *et al.*, 2019)
- Thermal (or vacuum) evaporation forms and grows thin coatings on solid materials' surfaces. During thermal evaporation, vaporized target material reaches the substrate with minimum hindrance (Mattox, 2010).
- Arc vapour deposition involves vaporizing a cathodic or anodic electrode with a high-current, low-voltage electric arc and depositing the evaporated material on a substrate. The substrate is biased to increase film ion transport, and the evaporated material is strongly ionized (Abegunde et al., 2019).
- Ion plating It bombards a film with atomic-sized energetic particles in an inert gas discharge system to modify and manage its characteristics. Plasma is produced via hollow cathode discharge. High-energy flux ions hit the substrate before and during thin film formation (Abegunde et al., 2019).

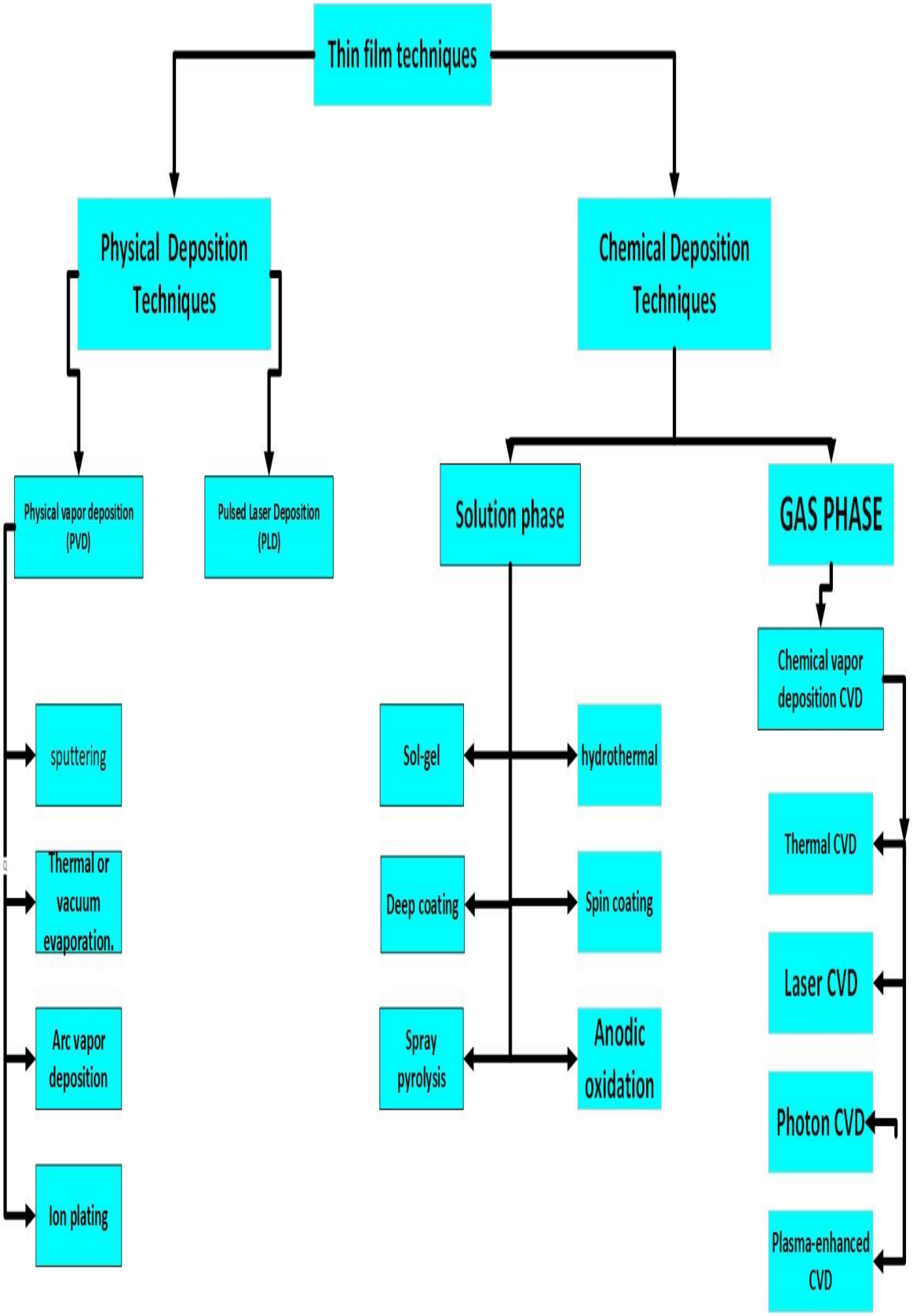

Figure 3.7. The techniques of thin films.

3.5.2. Chemical deposition techniques

These techniques are split into two groups, gas phase chemical vapor deposition (CVD) is a method that uses the interaction of a substrate with a volatile precursor to form a thin layer. A chemical reaction from vapor deposits the desired solid substance on a heated substrate surface. homogeneous thickness and small pore coatings can be created using the CVD technique. CVD demands a low vacuum, but not a high one (Stoian *et al.*, 2021). And the solution phase, includes the most vital techniques used to produce the thin films as shown below some techniques.

3.5.2.1. Hydrothermal method

This hydrothermal term refers to a heterogeneous reaction in which insoluble compounds are dissolved and crystallized at high pressure and temperature utilizing aqueous solvents or mineralizers. Solvents and starting ingredients are placed in a heat-resistant closed container and heated to the necessary temperatures in the hydrothermal process. The sort of solvent to be employed is what determines the method's distinctive name. The hydrothermal method uses water as a solvent, while the solvothermal approach uses alcohol or an organic solvent. Purification, change, dehydration, crystal development, degradation, extraction, reaction sintering, electrochemical reaction, mechanical chemical reaction, and other chemical reactions have all been produced using the hydrothermal process Figure 3.8 shows this method (Kudret, 2011; Demir, 2018).

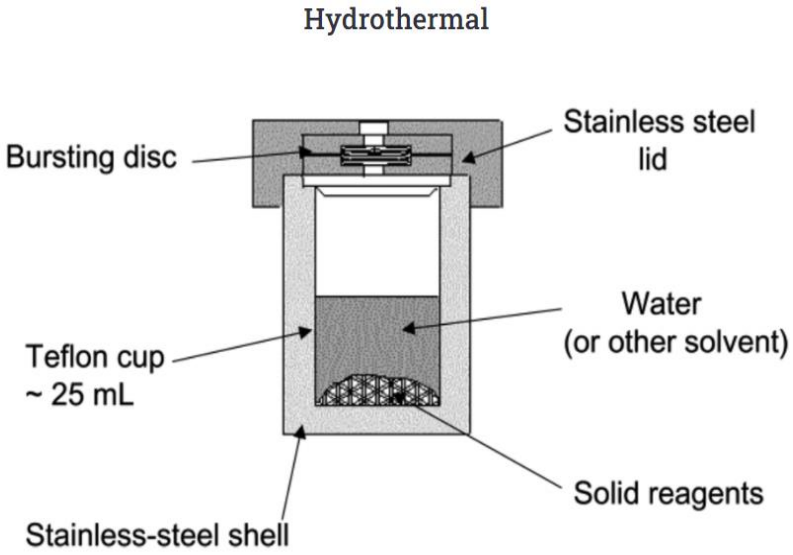

Figure 3.8. Hydrothermal system

3.5.2.2. Spray pyrolysis

Among thin film production technologies, spray pyrolysis is the simplest and most cost-effective. Spraying is far more favorable than other methods since it has a simple structure, requires less equipment, allows for intervention in the manufacturing process, and does not require a vacuum atmosphere for thin film creation. Spray pyrolysis does not need the use of costly materials or chemicals. Dense film deposition, porous film deposition, and powder production have all been accomplished using this technology. This adaptable approach can also be used to create multilayered films. Spray pyrolysis has been utilized in the glass sector and solar cell manufacturing for decades.

The spraying procedure involves combining the aqueous solutions that will be used to create the films and spraying them on the heated base by atomizing them with air or nitrogen gas. Spray pyrolysis typically consists of an atomizer, precursor solution, substrate heater, and temperature controller as shown in Figure 3.9. The film's quality is affected by experimental variables such as substrate temperature, sputtering rate, and film thickness. Simultaneously, experimental factors such as spray head size, the space length between the spray head and the substrate, and The pure water to acid solution ratio is critical in obtaining a high-quality film. The sprayed solution's drop size has a considerable influence on film quality (Perednis and Gauckler, 2005; Sönmezoğlu et al., 2012).

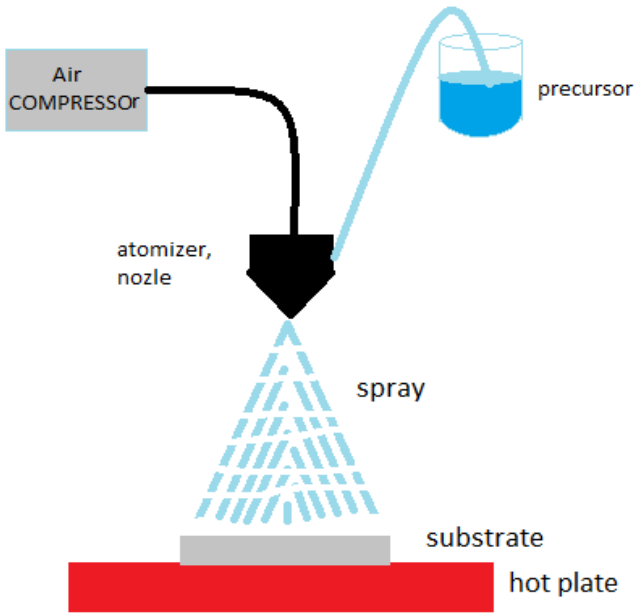

Figure 3.9. Spray pyrolysis system

3.5.2.3. Anodic oxidation

Anodization is an electrochemical oxidation process of increasing the thickness of the natural oxide layer on the surface of metals or semiconductors Al, Ti, Hf, W, Nb, Sn, Zr, etc… Figure 3.10 show the anodic oxidation system (Lee, 2010).

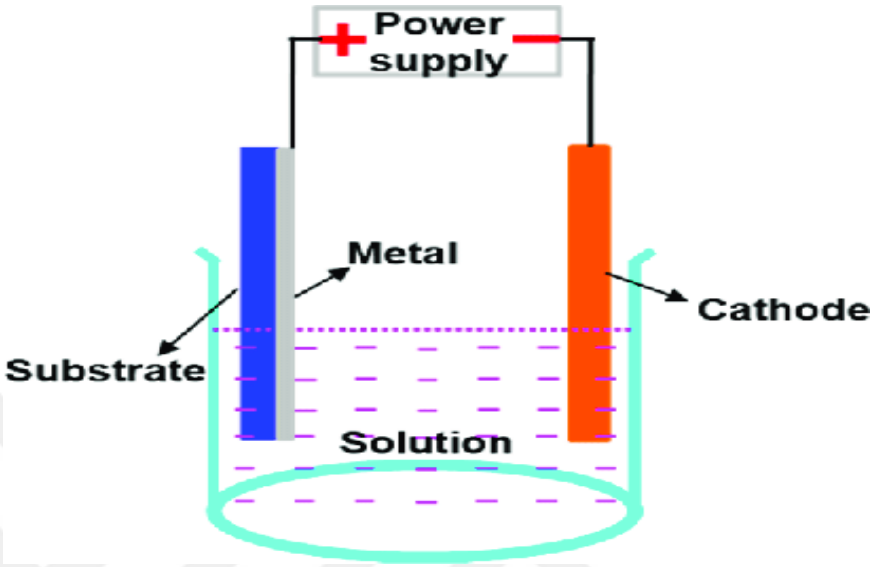

Figure 3.10. Anodic oxidation (Wang et al., 2018).

Anodization is a traditional metallurgical process for coating a metallic surface with a protective and attractive oxide deposit. Anodization is a process that evolved from electro-machining. This procedure can be used on any metal that is exposed to the elements. It thickens and densifies the oxide layer that has formed on the surface of metals. The anode is an anodized metal or alloy that is attached to the positive electrode of the power supply and immersed in a solution of electrolytes. The cathode, which is responsible for the release of oxygen, is typically constructed out of inert material such as platinum foil, graphite, or carbon. The reactions between the anode and cathode and in the electrolyte solution after the two electrodes are placed in the bath that has been pre-prepared with the appropriate electrolyte, anode oxidative degradation, metal particle migration, reduction of an ion to its zero valence state, particle creation and growth by nucleation, Stopping growth using capping agents, and 31 Processes like precipitation of particles as a consequence of which an oxide coating is formed on the substrate surface. The metals Pd, Ni, Co, iron, titanium, Ag, and Au are utilized to manufacture metal NPs of varying sizes (beginning at roughly 15 nm). The features of the resultant oxide film, such as nanoscale roughness, morphology, and surface chemistry, depending on a variety of process parameters, including applied electric field, current, solution composition, pH, and temperature (Mor *et al.*, 2006).

3.6. Formation Mechanism of TiO_2 Nanotubes

Anodization is an electrochemical method that forms a protective or decorative oxide deposit on the surface of a metal. Generally, anodization enhances both the thickness and density of the oxide layer generated on the surface of a metal exposed to the earth's atmosphere. The required anodization cell for this process is shown in the Figure 3.10. The conductive part to be anodized is placed in the electrolyte and it is linked to the positive terminal of the dc power source and served as the anode. Platinum plates or rods are generally used as cathodes (Grimes and Mor, 2009).

The color of the TiO_2 layer quickly changes during the process of anodization, going from a deep purple to blue, yellow, and green. The color variation is caused by an increase in the amount of TiO_2 present. Because of its propensity to produce soluble hexafluoro titanium complex, (F-) is a crucial factor in tubs structure creation ($[TiF6]^{2-}$). It also has a tiny ionic radius, which allows it to penetrate the emerging TiO_2 lattice. and be moved across the oxide by an applied electric field. Simply put, it's a dissolving agent for oxides. The reactions that lead to tubs nanostructure development are listed below :

Oxidation of TNT

$$Ti \rightarrow Ti^{4+} + 4e^{4-} \qquad (3.1)$$

Creation process of oxide layer

$$Ti^{4+} + 2H_2O \rightarrow TiO_2 + 4H^+ \qquad (3.2)$$

Dissolution the oxidation layer

$$TiO_2 + 6F^- + 4H^+ \rightarrow [TiF_6]^{2-} + 2H_2O \qquad (3.3)$$

The oxidation of Ti to Ti^{4+} is indicated by Eq. 1. According to Equation 2, H+ ions gathered throughout hydrolysis would lead F- ions to travel to H+ sites for electroneutrality, and F- may compete for O_2- sites in the oxide. Dissolution of TiO_2 happened when the amount of these ions achieved a threshold level in local locations, resulting in the production of $[TiF6]^{2-}$ (Eq. 3), Figure 3.11 clearly explained TNT's creation.

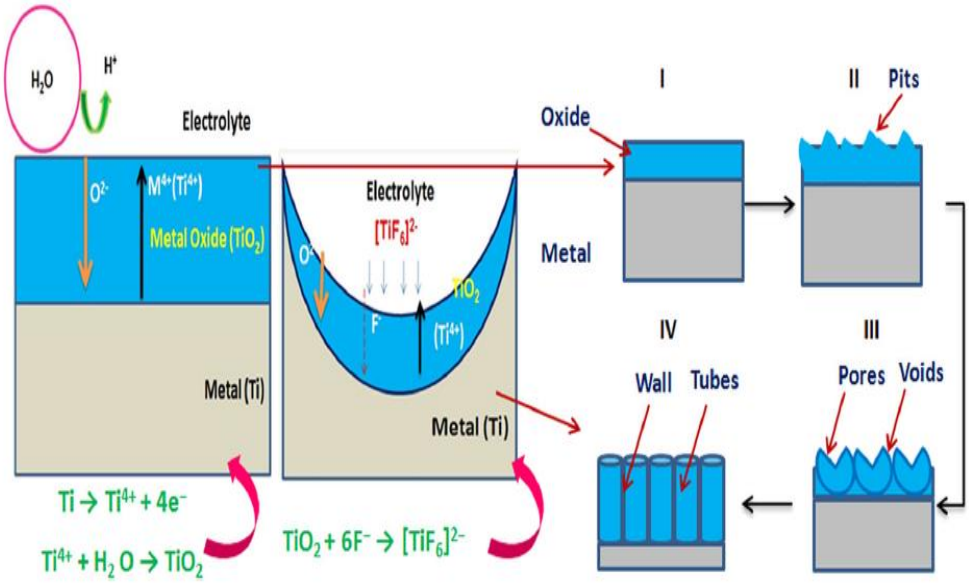

Figure 3.11. TNT's process of creation (Indira et al., 2015).

Nanopores formed on the oxide surface, as shown schematically in Figure 3.12. along with the current and time transition. Because the first little pores are so small, an amount of H+ At the base of the pore, where Ti was released from the metal and dissolved in the solution, ions are formed and the amount of HF inside the pores grows quickly. The wall of pores dissolves at high concentrations of HF until the surrounding pore walls vanish. Simultaneously, small pores' integration led to the formation of bigger pores. At the same time, increased electric field-assisted disintegration near the bottom of pores causes the pore to deepen and voids to form. The Ti–O bond changes as a result of the applied electric field (Indira *et al.*, 2015).

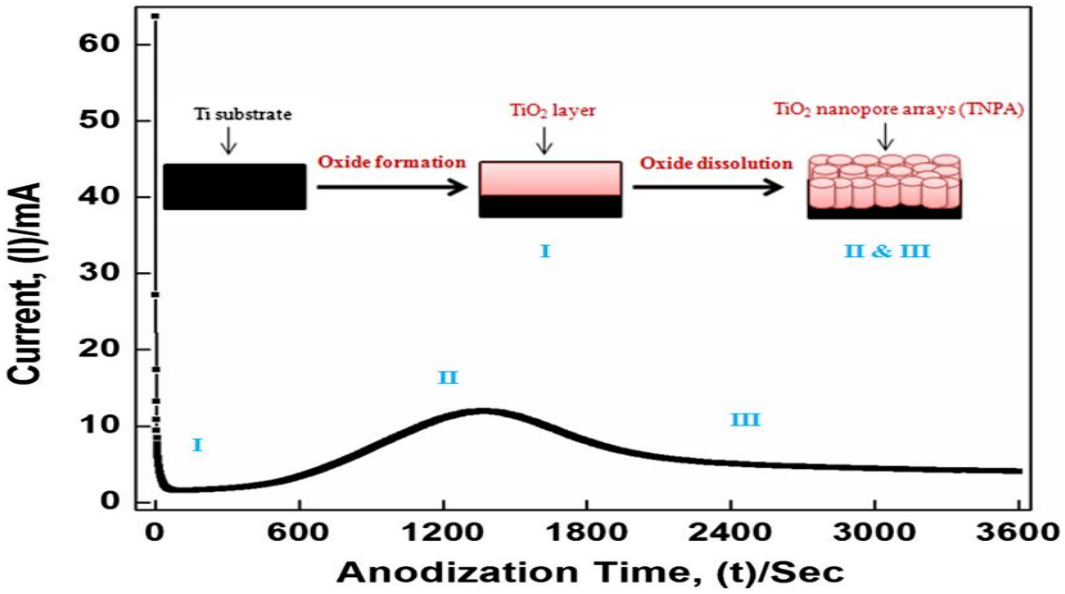

Figure 3.12. Shown schematically the Nanopore growth vs current-time transient (Indira et al., 2015).

3.7. Photocatalysis

Photocatalysis is a science that involves using a catalyst to accelerate chemical reactions using or requiring illumination. Photocatalysts are materials, usually a semiconductor, that are capable of absorbing enough energy (or a certain wavelength) of light to create reactive oxidizing species (ROS), which can result in the photocatalytic transformation of toxicants. This process creates electron-hole pairs, which allow reaction participants to undergo chemical changes, and regenerates the pollutant's chemical composition after each cycle of these interactions (Khan, Adil and Al-Mayouf, 2015).

The necessary band gap, appropriate shape, large surface area, stability, and reusability are all important characteristics of the photocatalytic system. Metal oxides with these properties, such as vanadium, chromium, titanium, zinc, tin, and cerium, go through similar main photocatalytic reactions, for instance, the absorption of light, which results in charge separation and the creation of positive holes capable of oxidizing organic substances (Khan, Adil and Al-Mayouf, 2015).

Several parameters influence photocatalytic activity, Pore structure, pore diameter, crystallinity, and structural dimension are all factors to consider. As a result, the most significant research subject in photocatalysis is improving photocatalytic performance by changing the mentioned parameters. Furthermore, TiO_2 nanospheres have good characteristics, distinct architectures, and are widely employed in a variety of applications . Furthermore, the structural aspect of this material is to improve light gathering capacities by enabling adequate light energy to pass through (Karthikeyan *et al.*, 2020).

The production of several linked semiconductors, including ZnO_TiO_2, CdS_TiO_2, and Bi_2S_3/TiO_2, has attracted a significant amount of interest in recent years. The synthesized couples improve photocatalytic efficiency by increasing the rate of recombination of photogenerated electrons and holes, and they could be used in several applications for instance photovoltaic systems, the splitting of water molecules, and the breakdown of organic matter. These nanocomposite materials were also thought to be potential materials for developing a high-efficiency visible-light photocatalyst. these composites are also capable of making up for the weaknesses of the parts individually, as a consequence, a synergistic effect is produced, which includes improved charge separation and photostability. As a result, visible light-driven coupled photocatalysts with the ability to break down organic matter are of tremendous interest (Pelaez *et al.*, 2012).

3.7.1. Photocatalytic degradation mechanism on TiO_2

It should be highlighted that for the effective formation of reactive oxidizing species, at least two events must occur concurrently during the photocatalytic process. Photogenerated holes oxidize dissociatively bound H_2O in the first process, while photoexcited electrons reduce an electron acceptor (typically dissolved oxygen) to form a hydroxyl and superoxide radical anion in the second (Pelaez *et al.*, 2012). The equations below show the degradation process :

$$TiO_2 + light \rightarrow TiO_2\,(e^- + h^+) \quad (3.4)$$

$$H_2O + h^+_{vb} \rightarrow OH^* + H^+ \quad (3.5)$$

$$O_2 + e^-_{cb} \rightarrow O_2^{\cdot -} \quad (3.6)$$

$$OH^* + \text{pollutant} \rightarrow H_2O + CO_2 \quad (3.7)$$

$$O_2^{\cdot -} + \text{pollutant} \rightarrow CO_2 + H_2O \quad (3.8)$$

$$O_2^{\cdot -} + H^+ \rightarrow OOH \quad (3.9)$$

$$OOH + OOH \rightarrow H_2O_2 + O_2 \quad (3.10)$$

$$OOH + \text{pollutant} \rightarrow CO_2 + H_2O \quad (3.11)$$

In the process of photocatalysis, an electron is moved from the valence band to the conduction band when the energy of the incident light is greater than the band gap of the semiconductor Figure 3.13 shows that process. Since anatase TiO_2 has a band gap of 3.2 eV, ultraviolet light that has a wavelength of 387 nm is needed. When a photon is absorbed by an electron, it causes the electron to be stimulated to the conduction band (eCB), which then creates a positive hole in the valence band (hVB+). Charge carriers may be contained as Ti3+ and O defect sites in the TiO2 lattice, or they can recombine and lose energy. Charge carriers may also migrate to the surface of the catalyst and initiate redox reactions with adsorbates. Positive holes on the surface may oxidize OH or water to generate OH radicals, which are very powerful oxidants. Hydroxyl radicals

can oxidize organic molecules, which leads to the formation of mineral salts, CO_2, and water during the mineralization process (Yeskel,. 2021).

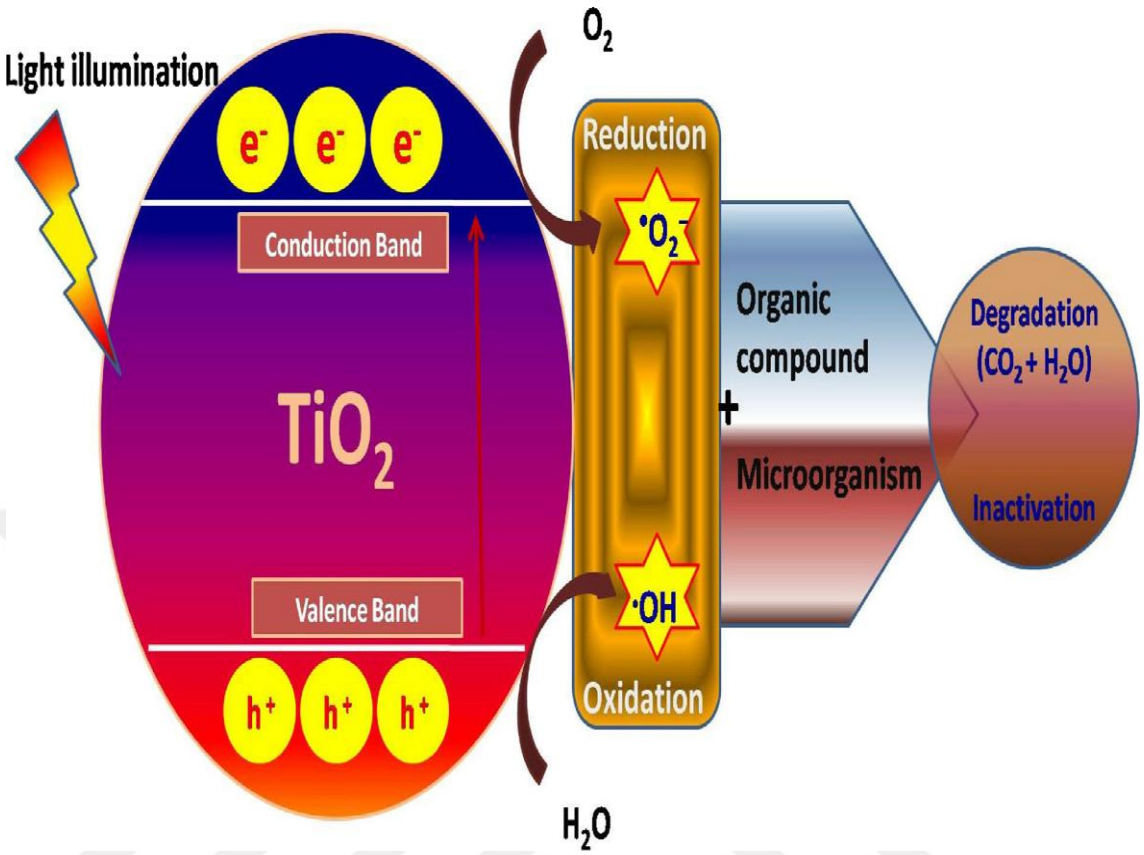

Figure 3.13. Schematic of TiO_2 photocatalytic mechanism (Prakash et al., 2018).

4. MATERIALS AND METHODS

In this work, it was aimed to produce (CTS_TNT) films by producing Cu_2SnS_3 nanolayer / TiO_2 nanotube hybrid nanocomposite. The creation of TiO_2 nanotubes using an electrochemical technique using a Ti plate as the basis, followed by spray pyrolysis to add a Cu_2SnS_3 nanolayer. The TiO_2 / Cu_2SnS_3 nanocomposite that resulted in its photocatalytic activity was investigated. Figure 4.1 shows the steps of production for this composite structure.

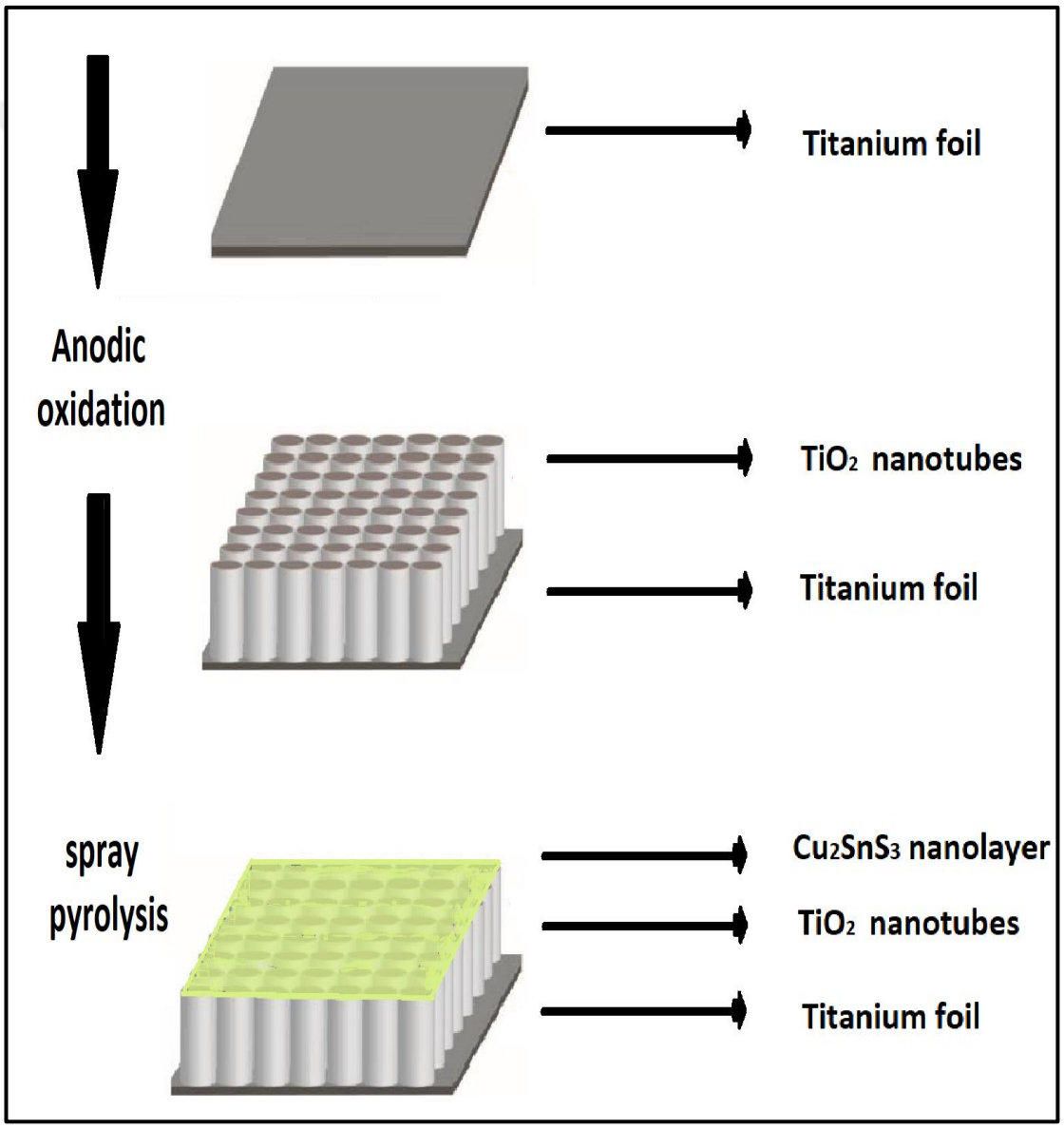

Figure 4.1. Production process of CTS/TNT films

4.1. Preparation of The TiO_2 Nanotube Samples

At the first, titanium foil was cut 0.9 – 4 cm (0.25 thickness, 99.7% purity, Sigma Aldrich). Then, the cut pieces of titanium foil were cleaned in an ultrasonic bath for thirty minutes, respectively, with acetone, 2-propanol and deionized water. CH_3COCH_3 (Acetone) and $CH_3CH(OH)CH_3$ (2-propanol) were used in the cleaning process. After the cleaning process, the titanium foils pieces were dried with nitrogen gas and made ready for anodic oxidation. The ultra sonic bath used in cleaning process is shown in Figure 4.2.

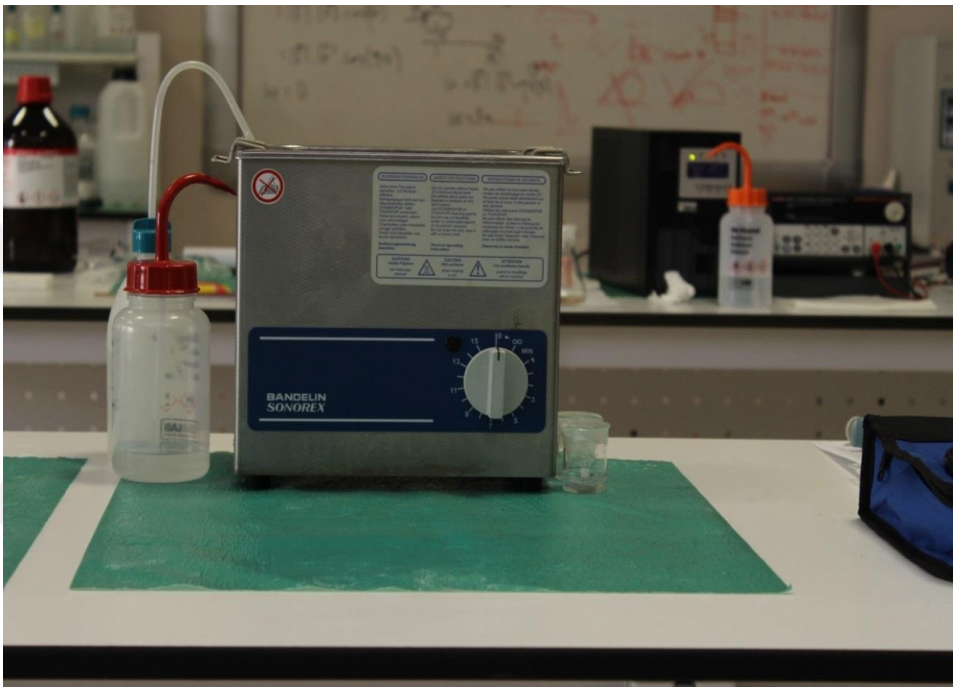

Figure 4.2. Ultrasonic bath that used in cleaning process

TiO_2 nanotubes were obtained by anodic oxidation method. First of all, the tools that were used along the production process were cleaned with alcohol and left in the oven for drying. To remove any external elements, then, electrolyte solution was prepared for the anodic oxidation process. 0.4 gr (0.4% wt.) Ammonium Fluoride (NH_4F) (98% purity, Sigma Aldrich), 5 ml (5% wt.) deionized water and 85 ml (94.6% wt.) Ethylene Glycol (% 99.8 purity, Sigma Aldrich) containing electrolyte solution is prepared and filled into a Teflon container, in order to make this solution homogeneous and well mixed it was left for 15 minutes at 1000 rpm in the magnetic stirrer as shown in Figure 4.3.

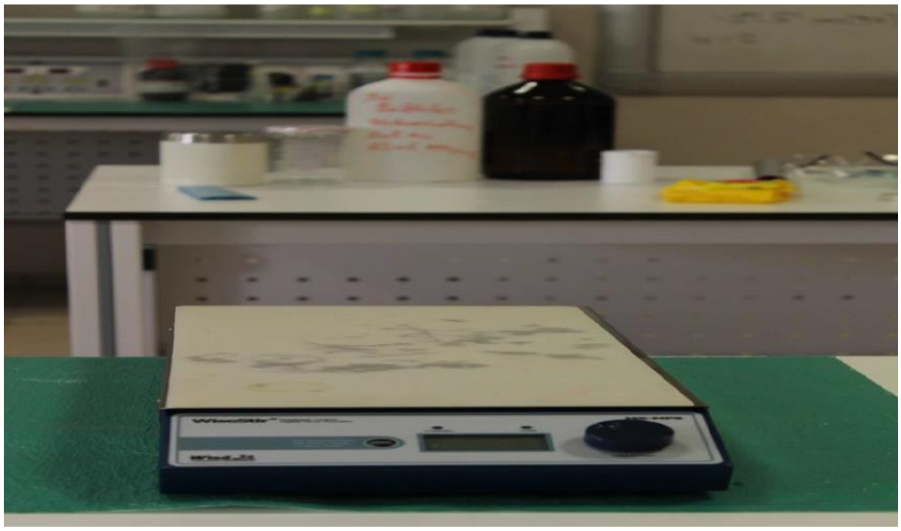

Figure 4.3. Magnetic stirrer

At the end of this process, the experimental setup was set up the Ti Plate to the anode (+) and Pt was connected to the cathode (-), in addition the distance between them was adjusted to be 2.5 cm; and parallel, the speed of the magnetic stirrer was set to 600 rpm and the temperature at 35 ^{o}C as shown in Figure 4.4. Thus, the equality of fluorine ion distribution was ensured during the experiment. The anodization process, which will be continued for 3 hours, by increasing the power supply voltage up to 30 V by increasing 2 V per second, the formation of TiO_2 nanotube arrays (TNT) was achieved.

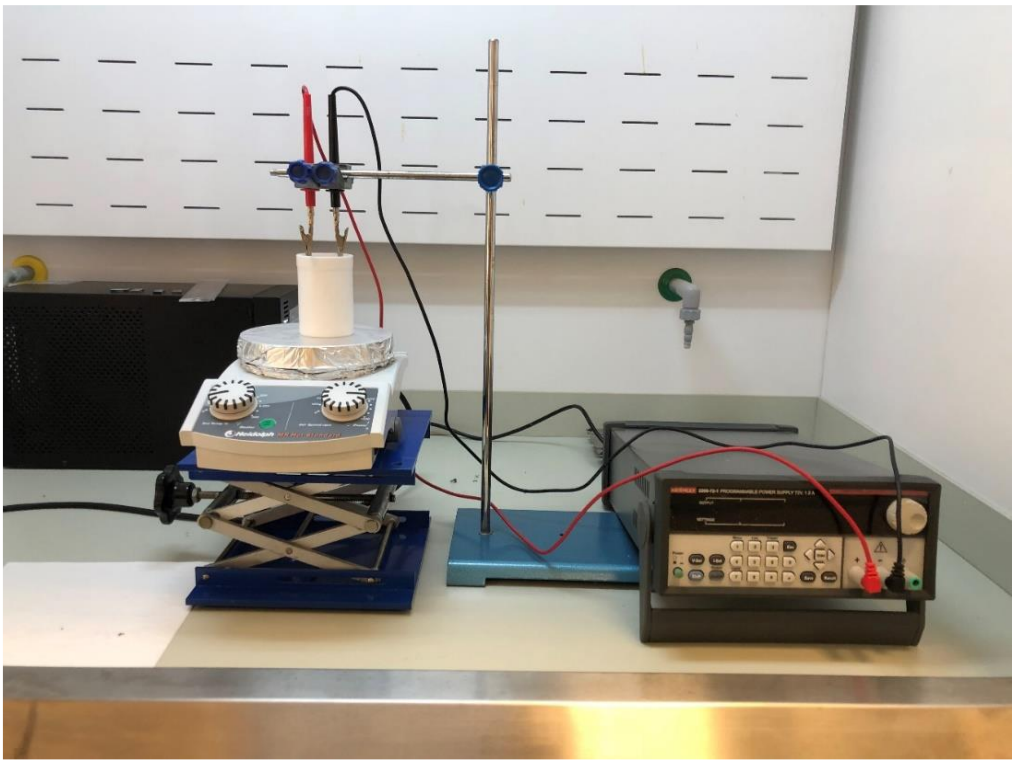

Figure 4.4. Anodization setup

The nanotube was washed in an ultrasonic bath of Methanol (CH4O, 99.8% purity, Sigma-Aldrich) for 2 minutes after being extracted from the electrolyte liquid at the end of the anodization process to eliminate residues on its surface. The nanotube was dried using nitrogen gas after it had been cleaned. Figure 4.5 shows the formation mechanism of TNDs in the anodic oxidation process.

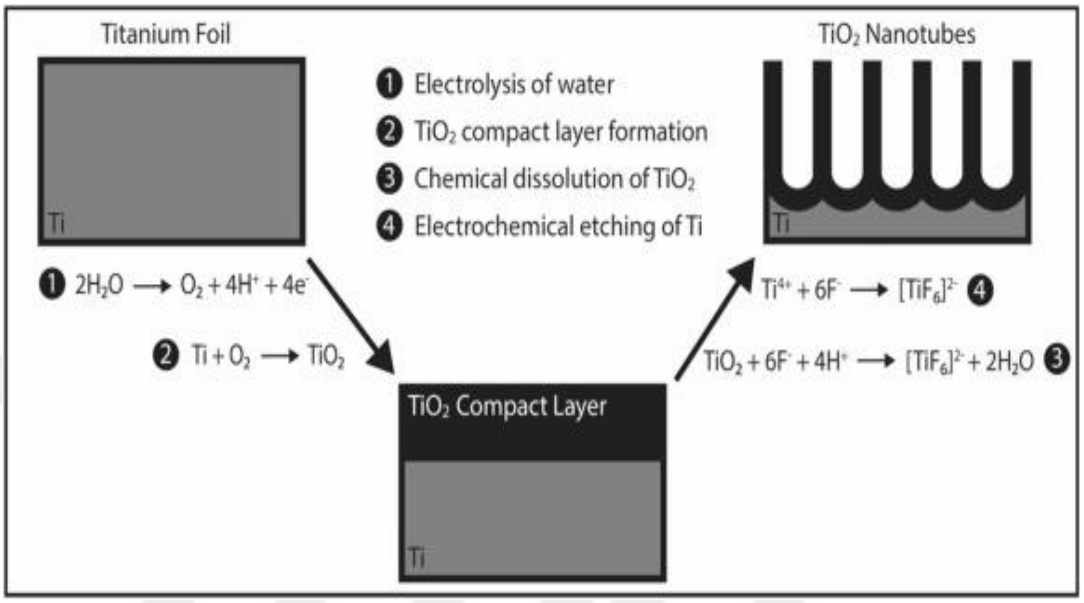

Figure 4.5. Formation mechanism of TiO_2 nanotube arrays (Çırak et al., 2017).

TNT produced at the end of the previous operations was changed to Anatase form by annealing at 450 °C for 1 hour in air in s special furnace shown in Figure 4.6 and the Figure 4.7 illustrates a graph of temperature change over time during TNT annealing.

Figure 4.6. Used furnace for annealing the TNT

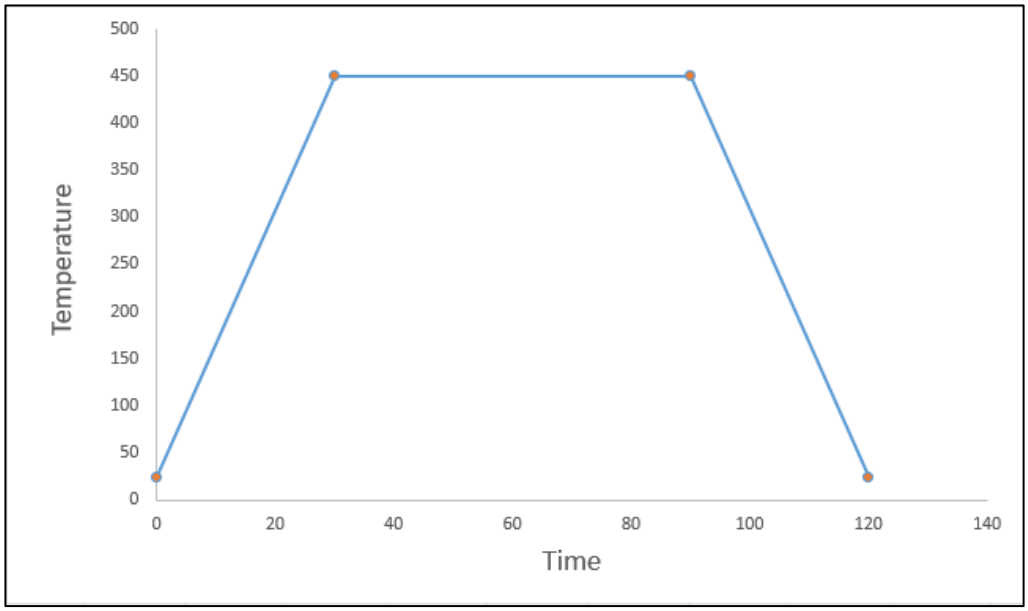

Figure 4.7. Time variation of temperature during annealing of TNT

4.2. Preparation of CTS_TNT Composite By Using Spray Pyrolysis Method

The coating solution is made up of copper (II) Nitrate Cu $(NO_3)_2$ • H_2O 0.025 M, tin (II) chloride dihydrate $SnCl_2$ • H_2O (98 % purity, Alfa Aesar) 0.01 M, and thiourea Ch_4N_2S (98 % purity, Alfa Aesar) 0.2 M. As well as hydrochloric acid HCl 25µl to dissolve the solution well. Also, by filling a closed plastic container with deionized water up to 40 ml the solution can be completed. and putting it in the ultrasonic bath for 10 minutes and the mixture device for 3 minutes as shown in Figure 4.8 to homogenize the solution well.

Figure 4.8. The mixture device

Then, with a distance of 20 cm from the nozzle to the sample, and utilizing the air compressor, which was controlled by the pneumatic control system as shown in Figure

4.9, whose spray flow rate had been adjusted to 6 ml/min as shown in Figure 4.10. spraying duration was 3, 5, and 7 minutes, respectively, on the pre-heated TNT 500 c. The sample is ready to check after the end of the spraying period.

Figure 4.9. Air pressure control device

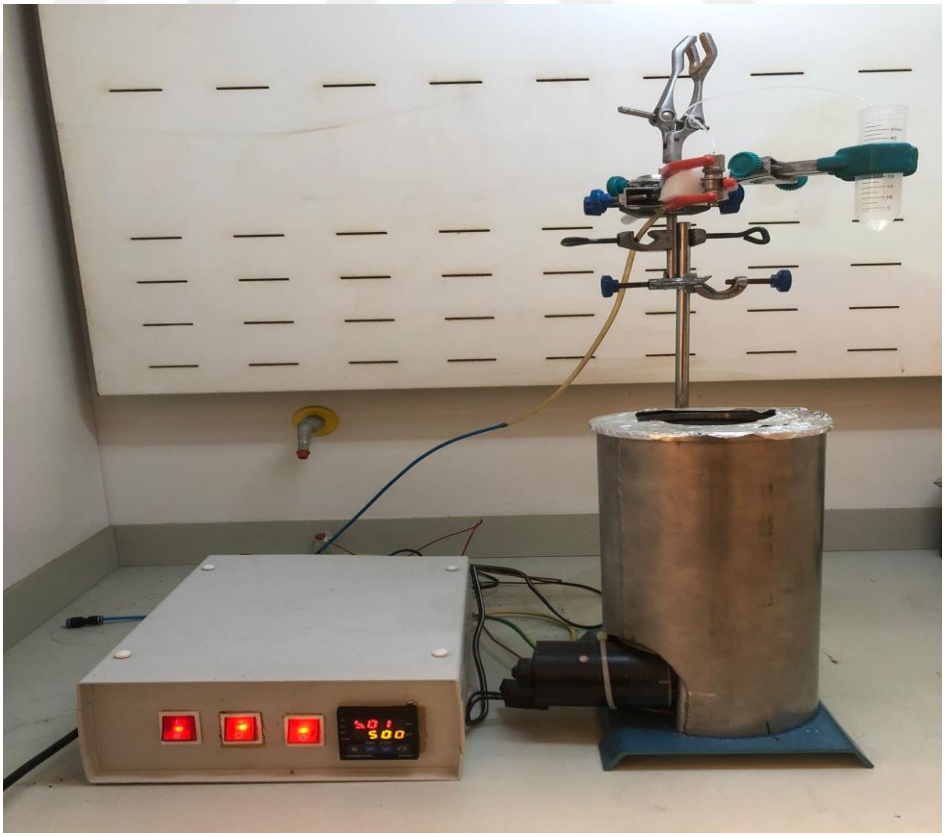

Figure 4.10. The system of spray pyrolysis coating

4.3. CTS_TNT Photocatalytic Performance Tests

The photocatalytic activity of CTS/TNT nanocomposite films was examined using Rhodamine B photodegradation. The nanocomposite film was immersed in a quartz cuvette containing RhB dye 3 ml solution and left in the dark for 30 min , it was exposed to a UV light source (100W, 365 nm) and a visible light source, which was placed 10 cm away from the source, the sources are shown in Figure 4.11.and 4.12. After the solution reached adsorption/desorption equilibrium in the dark environment, the source lamp was put in front of the RhB solution. Then, by switching the lamp on, a photocatalytic reaction was initiated

The photocatalysis activities of the CTS_TNT nanocomposites were tested with the 555 nm wavelength absorbance value of RhB by UV-Vis spectrophotometer (PG Instruments, T80 +) as shown in Figure 4.13 for predetermined time intervals.

Figure 4.11. UV source

Figure 4.12. Solar simulator, visible light

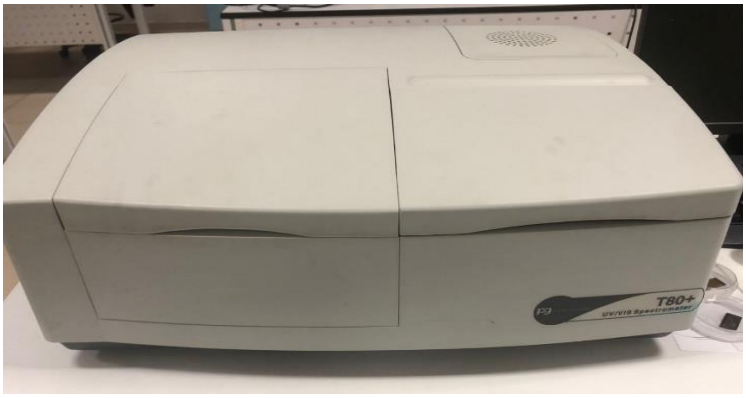

Figure 4.13. UV-Vis spectrophotometer

4.4. Characterization

4.4.1. XRD (X-ray diffraction)

The formed CTS_TNT nanocomposites were analyzed utilizing Cu-K_α radiation (λ=1,5406 Å, 45 mV and 40 mA) with a 2° rotation speed between 10°-90° angles with an X-Ray diffractometer (XRD) (PANanalytical, Empyrean) as shown in Figure 4.14 in the Erzincan Binali Yıldırım University Basic Sciences Application and Research Center.

Figure 4.14. X-Ray diffraction device

4.4.2. Scanning electron microscope (SEM) and Energy dispersive X-ray spectroscopy (EDX).

The surface morphology of CTS/TNT nanocomposites formed at different spray duration were analyzed, as well as EDX is used to identify the elemental composition of any sample. EDX is a method commonly used in SEM devices and elemental analysis is performed by sending an electron beam on a sample using Field Emission Scanning Electron Microscopy (FESEM, FEI Quanta 450) as shown in Figure 4.15 in Erzincan Binali Yıldırım University Basic Sciences Application and Research Center.

Figure 4.15. Field Emission Scanning Electron Microscopy (FESEM)

5. RESULTS AND DISCUSSION

5.1. Cu_2SnS_3 Nanolayer / TiO_2 Nanotubes Nanocomposite Characterization

5.1.1. Morphological characterization

A field emission scanning electron microscope (FESEM, FEI Quanta 450) was used in order to examine the surface morphology of TiO_2 nanotubes and CTS_TNT nanocomposite films. As shown in Figure 5.1 on the surface of Ti foil the arrays were formed by anodic oxidation and the Diameter of TiO_2 nanotubes (arrays) was ~90 nm, length was ~4 μm (Çırak *et al.*, 2019) . The amount and size of CTS increased with increasing the time of coating or spraying. TiO_2 nanotubes and CTS nanolayer can appear together in surface images up to 3 and 5 minutes of spray coating as shown in Figures 5.2 and 5.3. But when the spraying goes up 7 minutes the CTS covered the nanotubes entirely as shown in Figure 5.4. Additionally, the CTS combination concentration was steady along all three samples. The CTS combination concentration was steady along all three samples. From the Sem Figures, it's clear that as the coating time goes up, the CTS starts to fill the tubes and forms a thin layer on the tubes' surfaces. Also, the tubes shouldn't have been coated completely with CTS in order to benefit from the synergistic between TiO_2 and Cu_2SnS_3 in degrading the pollutants. Figure 5.5 shows cross section image for 7 minute coated film which is indicated the CTS thin layer was ~ 6 nm

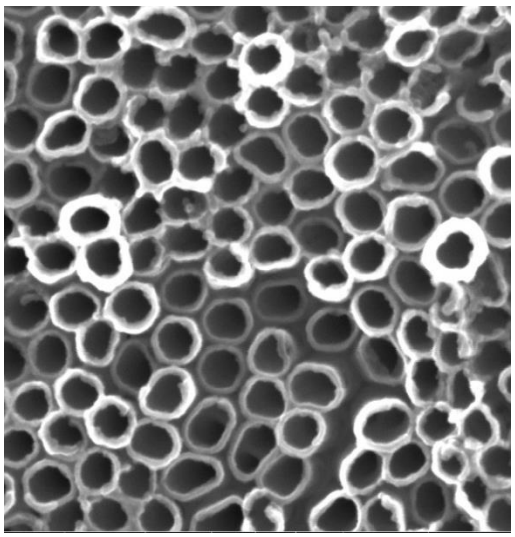

Figure 5.1. Bare TNT

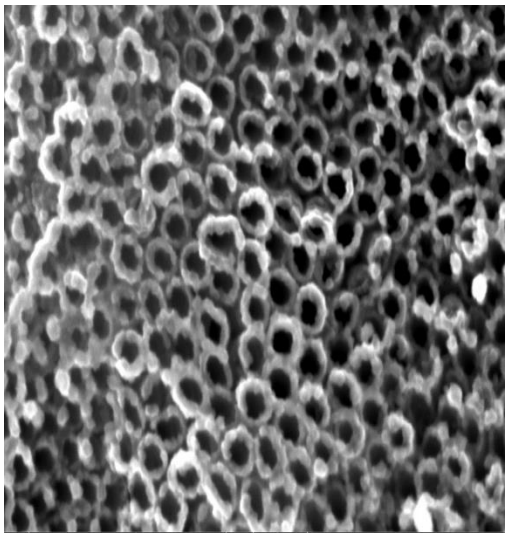

Figure 5.2. CTS_TNT_3 minutes

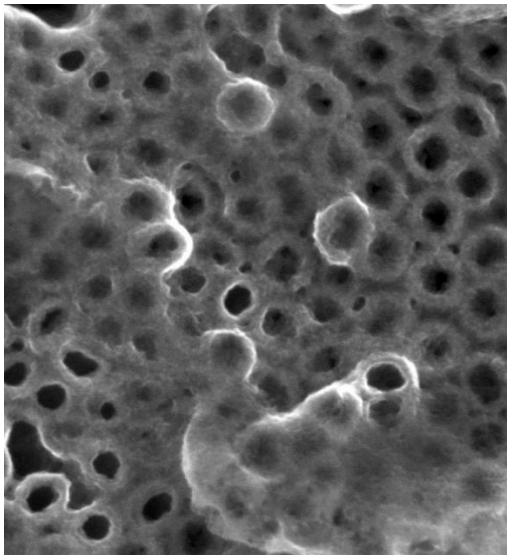

Figure 5.3. CTS_TNT_5 minutes

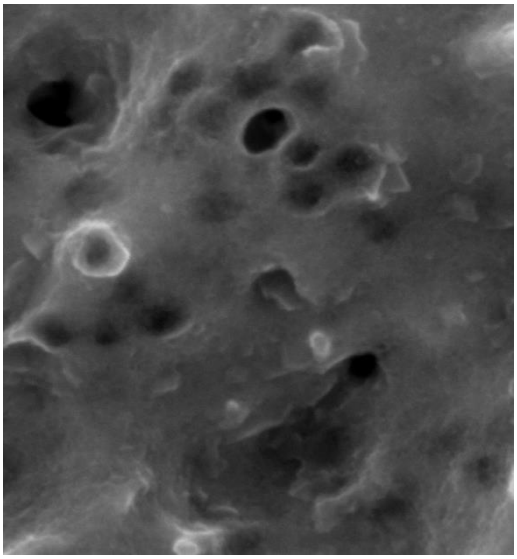

Figure 5.4. CTS_TNT_7 minutes

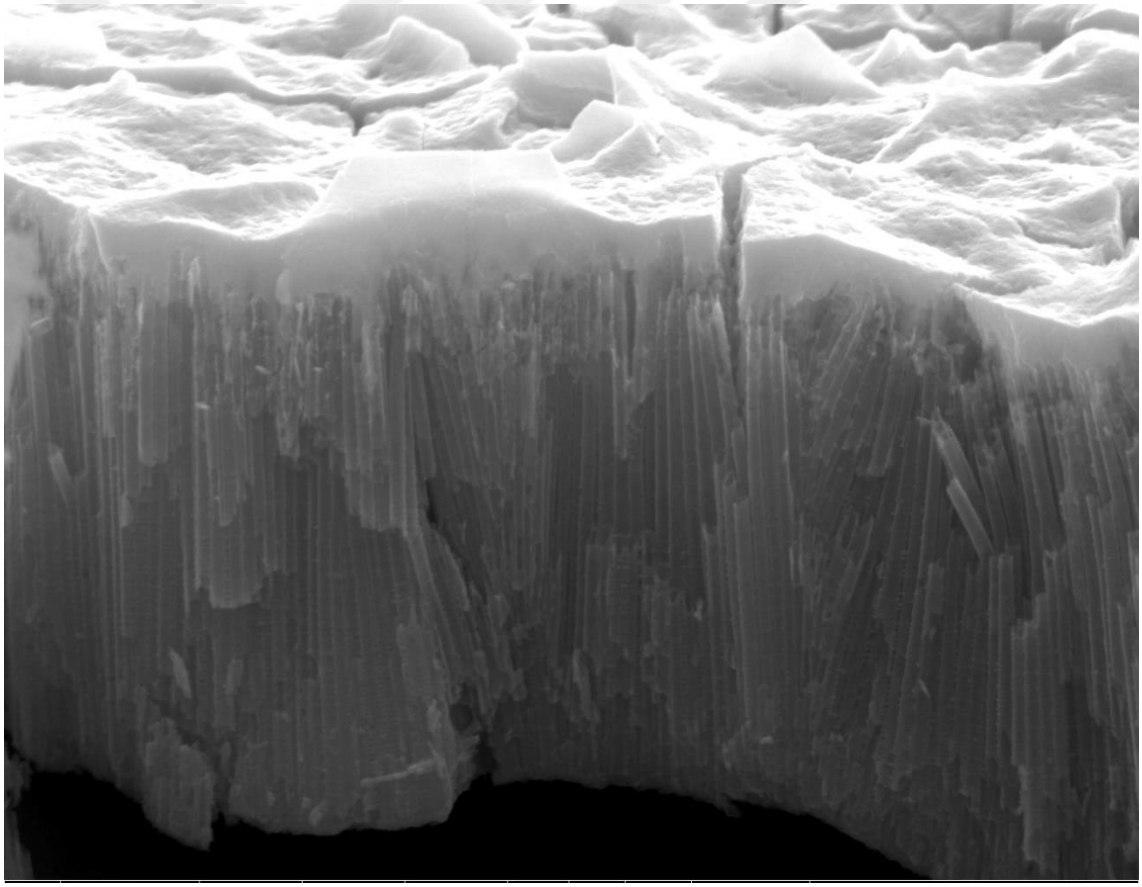

Figure 5. 5. Cross section of CTS_TNT_7 minutes

5.1.2. Crystallographic characterization

X-ray diffraction used to check the crystal structure of the films TNT and CTS_TNT. Figure 5.6 shows the patterns of films, diffractions at 25.3°, 37.9°,48.1°, 54.1°, 55.2° and 63.5° are matches with planes (101), (004), (200), (105), (211) and (204) planes of anatase TiO2 (JCPDS No. 21-1272), respectively. The other originated peaks belong to foil (T). The peak of Cu_2SnS_3 at 28.53^0 is corresponded to the plane (112) (JCPDS no. 89-47). As seen in Figure 5.6 , when coating time is 3 min, the Cu_2SnS_3 diffraction peak intensity is difficult to observe because of the tiny particle size and low coating, the Cu_2SnS_3 diffraction peak is difficult to observe. Also, Even though these intensity peaks were small but gradually started to appear with rising coating time, indicating bigger crystal sizes and enhanced crystallinity of Cu_2SnS_3 nanostructures.

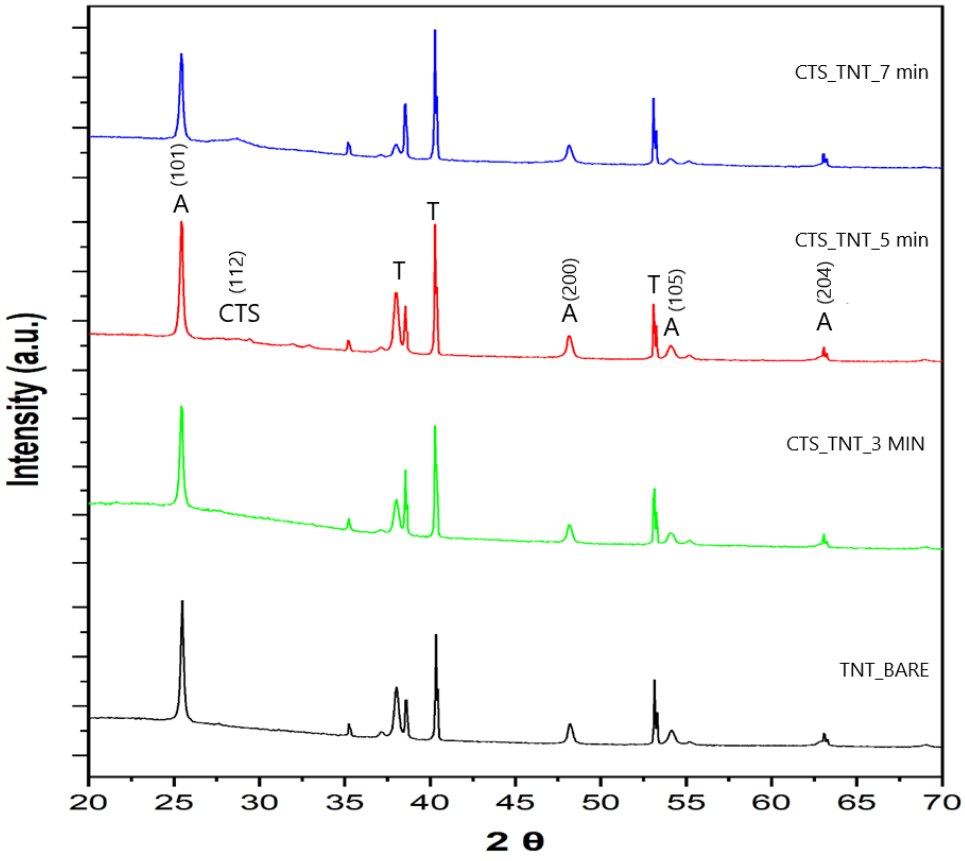

Figure 5.6. XRD patterns of TNT bare, (CTS_TNT_3 min), (CTS_TNT_5 min) and (CTS_TNT_7 min). A: anatase and T: titanium.

5.2. Photocatalytic Degradation Tests

Prepared TiO_2 nanotubes were coated with Cu_2SnS_3 by spray pyrolysis method in different coating times 3, 5 and 7 minutes were named according to coating duration respectively (CTS_TNT_3 min), (CTS_TNT_5 min) and (CTS_TNT_ 7 min), these samples were used as a catalyst to degrade the pollutant.

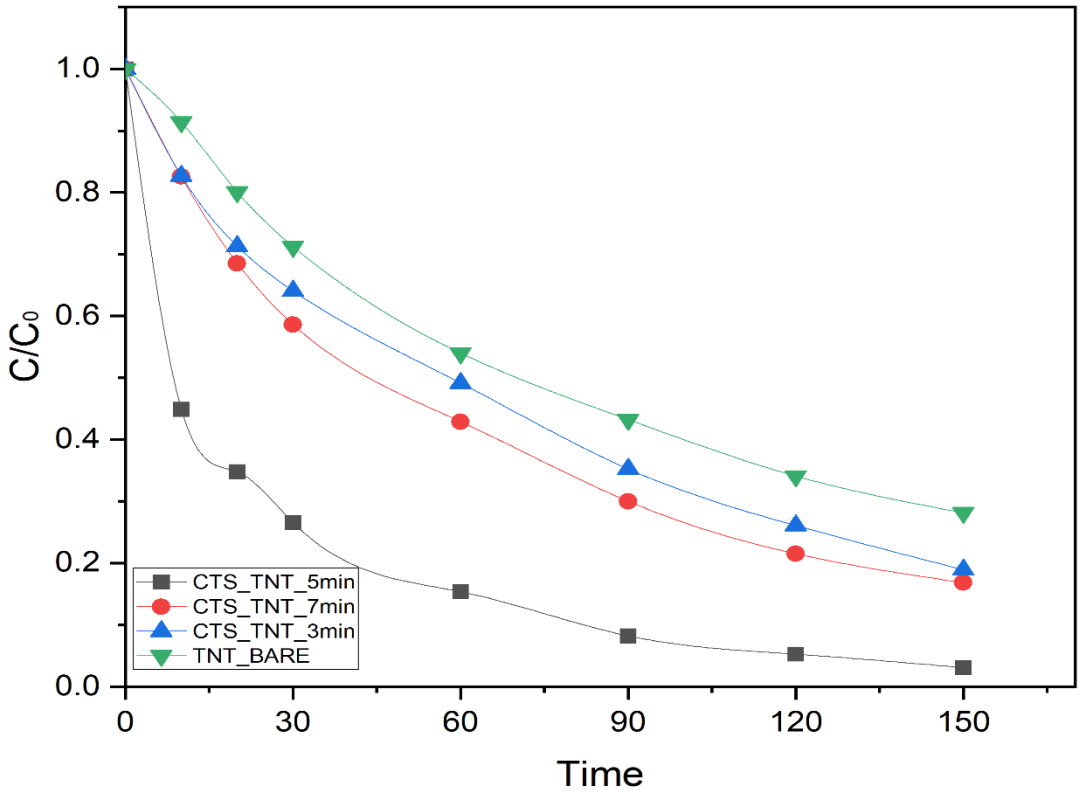

Figure 5.7. Photodegradation of RhB under UV light by bare TNT, (CTS_TNT_3min), (CTS_TNT_5 min) and (CTS_TNT_7 min) films.

According to Figure 5.7 TNT bare films degradation performance percentage is estimated at 65 %. Whereas, in the presence of (CTS_TNT 3min), the percentage photodegradation of RhB dyestuff was 78 % with increasing the duration time the films (CTS_TNT_5 min) percentage photodegradation was 98 % which is considered the best film performance among all the films. However, at the film (CTS_TNT 7 min) the performance was decreased to 80 % when the duration coating was 7 min probably because the tubes were filled with CTS. By using 5 minute coating time, the degradation performance of a bare TNT array was boosted by approximately 40%. This status demonstrates how the combination of TiO_2 and Cu_2SnS_3 improved the photodegradation activity of (CTS_TNT) films. This promoting influence might be the result of Cu_2SnS_3 nanoparticles being used to improve the active sites on TiO_2, which

raises the chances that OH* radicals and superoxide* radicals will form on the surface of (CTS_TNT).

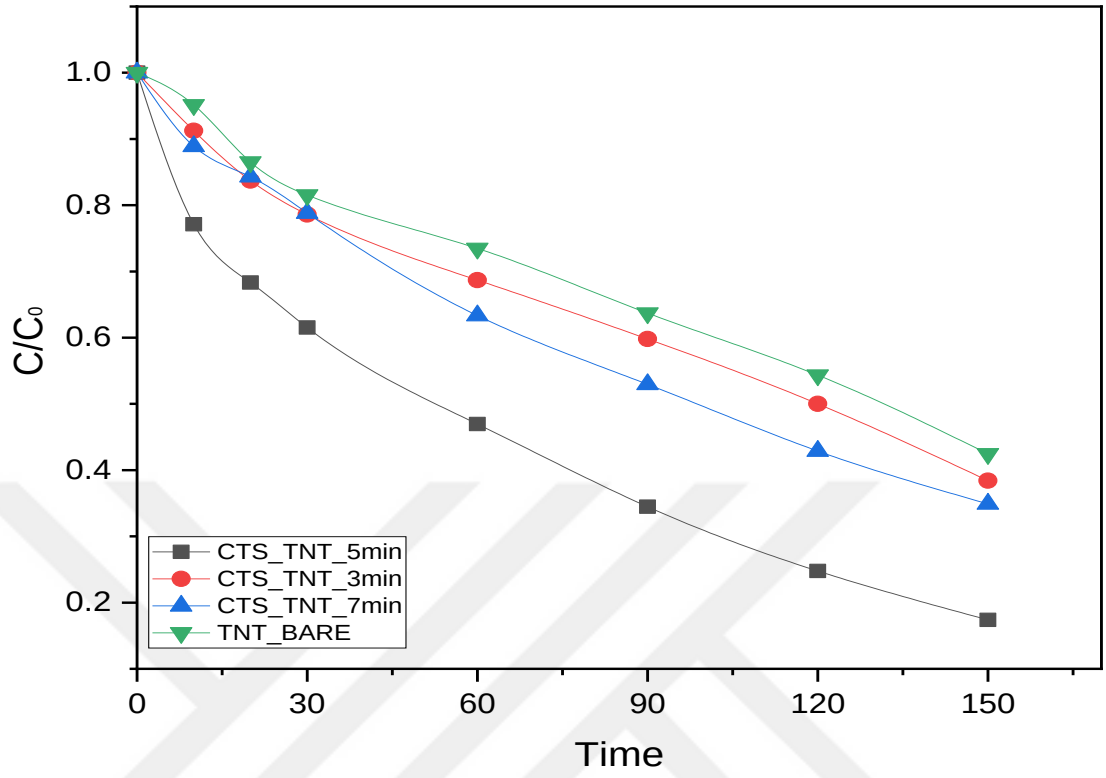

Figure 5.8. The degradation of RhB under visible light by bare TNT (CTS_TNT 3min), (CTS_TNT_5 min) and (CTS_TNT_7min) films.

In order to compare the performance of photocatalysis, the degradation of RhB by TNT bare and (CTS_TNT) was performed under visible regions, according to Figure 5.8. the percentage degradation of RhB on all the samples were , TNT bare 30 % ,(CTS_TNT_3 min) 70 %, (CTS_TNT_5 min) 80 % and (CTS_TNT_7 min) 75 %.

The results for the two figures indicate the same order of performance of the samples, however, the samples under UV exhibited better performance the reason is the UV photons have higher energies than visible light photons, Figure 5.9 shows the comparison between the two status UV and visible light.

The reusability of photocatalyst materials is a vital issue of dye and toxic molecule degradation to reduce the cost and the efforts. To evaluate the reusability of the photocatalyst, RhB was photodegraded by (CTS_TNT) for four repeated cycles as seen in Figure 5.10. After each successive exposure to light, the CTS TNT film has shown a high degree of photostability and high reusability potential. A minor reduction in the

effectiveness of the degradation could be attributed to Cu_2SnS_3 dissolving by the process of photo-corrosion or separation of Cu_2SnS_3 nanoparticles from the TNT.

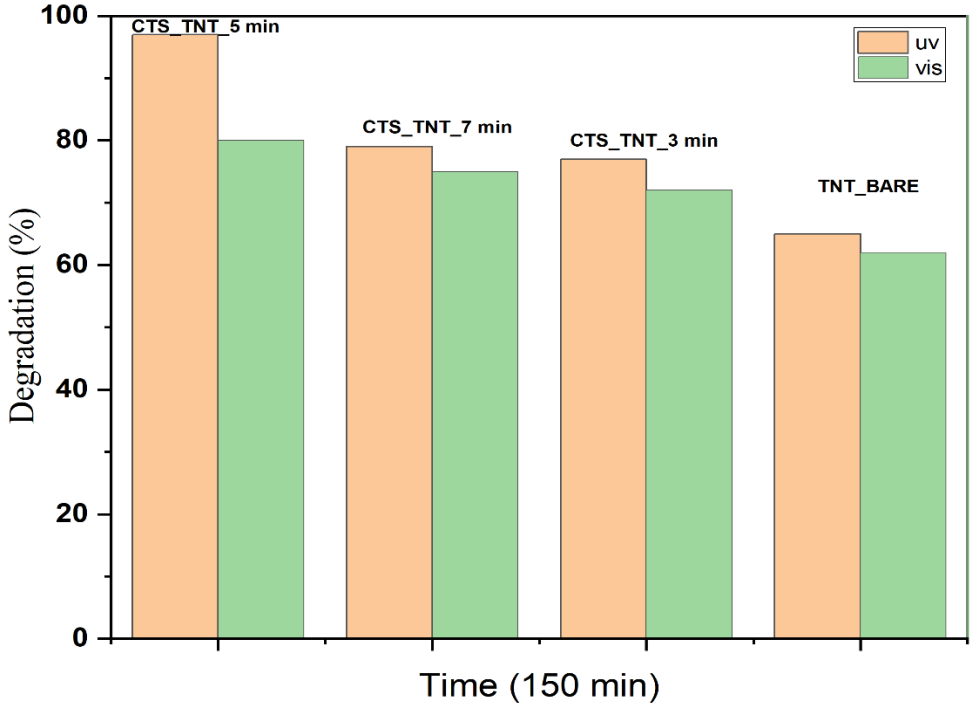

Figure 5.9. Comparison of photodegradation performance percentage under visible and UV light.

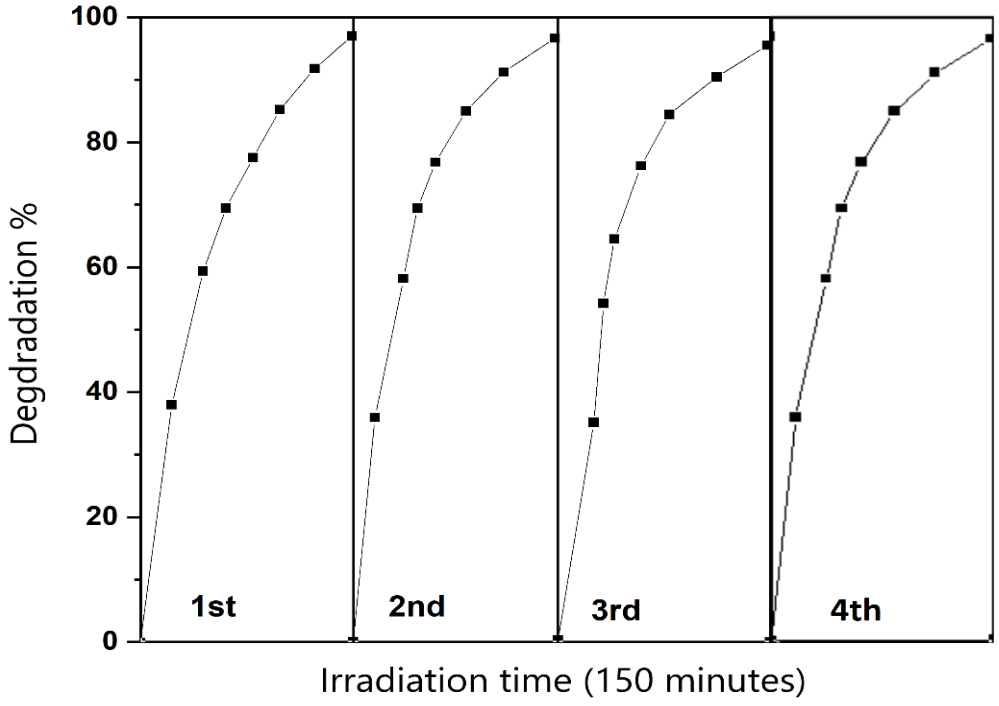

Figure 5.10. Photostability tests of (CTS_TNT_5min) by photodegradation of RhB under UV light.

5.3. Structural Analysis

Electron diffraction X-ray analysis (EDX) was used to examine the elemental composition of CTS-coated TNT thin films. In addition, the elements of the nanolayer on the tube's surface will be investigated. Figure 5.11 depicts the EDAX result of the CTS_TNT nanocomposite. The elemental analysis indicates the existence of a CTS nanolayer on the TNT surface, according to Table 5.1, the element ratios of CU, S, SN, O, and Ti in the total area of CTS_TNT nanocomposite are 4.35, 3.22, 2.5, 24.57, and 65.17%, respectively. These findings confirmed the low existence of Cu, Sn, and S atoms in the CTS_TNT photocatalysts.

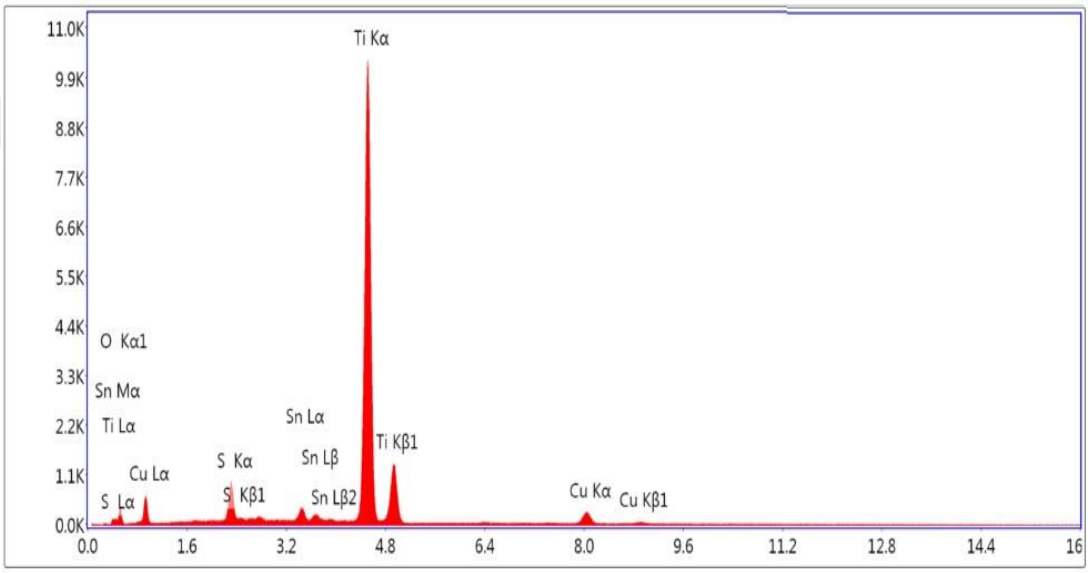

Figure 5.11. EDX spectra of (CTS_TNT_5 min) film.

Table 5.1. Percentage of presence of elements by EDX.

Element	Weight %	Atomic %	Net int	Error %
O	24.57	49.94	57.06	11.82
S	3.22	3.24	169.7	6.7
Sn	2.5	0.68	68.93	13.11
Ti	65.17	43.92	2958.38	1.32
Cu	4.35	2.21	92.42	6.6

5.4. Degradation Kinetic of RhB on CTS_TNT

The degradation kinetic of the RhB dyestuff solution on CTS_TNT was determined with the use of the pseudo-first-order reaction kinetic model, and the experimental data were utilized to determine how well this model fits the data using the following Equation

$$-\ln\left(\frac{C_t}{C_0}\right) = K_{app} \times t \quad (5.1)$$

In the equation that was just presented, C_t and C_0 stand for the concentration of dye at various irradiation times and the concentration of dye immediately before irradiation, respectively. The apparent pseudo first-order rate constant, denoted as k_{app}, was determined by taking the slope of the linear fitting graph of -ln C_0/C_t vs time (t). Figure 5.11 and 5.12 indicates that the photocatalysis of RhB dyestuff follows the pseudo-first order reaction kinetic for all CTS_TNT films with varying time coating. These data in reaction kinetics are similar to earlier research (Çırak *et al.*, 2019; Caglar *et al.*, 2021). Table 4 shows the apparent rate constants and correlation coefficients of all the samples under UV and visible light obtained for dye degradation processes from slope figures.

Table 5.2 Apparent pseudo first-order rate constants (k_{app}), and correlation coefficients (R-square).

Table 5.2. Apparent pseudo first-order rate constants (kapp), and correlation coefficients (R-square).

	K_{app}		R-square	
	Visible	UV	Visible	UV
TNT	0.0053	0.0085	0.9868	0.9919
CTS_TNT_3 min	0.0058	0.0106	0.9879	0.9954
CTS_TNT_5 min	0.0108	0.0209	0.9920	0.9614
CTS_TNT_7 min	0.0068	0.0117	0.9983	0.9897

The coating duration of the spraying has a considerable impact on the apparent rate constants and the degradation rate of RhB. As shown in Figure 5.12 and 5.13.

According to the findings in Table 5.2 the apparent rate constant and correlation coefficients of the samples steadily improve as the time coating increases. The biggest k_{app} and reaction rate achieved for (CTS _TNT _5 minute) under both UV and visible irradiation. In addition, k_{app} of (CTS _TNT_ 5 minute) under UV irradiation bigger than under visible irradiation. Furthermore, according to R-square data, k_{app}, which is the slope of the linear fitting graph under visible light fitted better in comparison with UV irradiation, but the reaction rate under UV was faster.

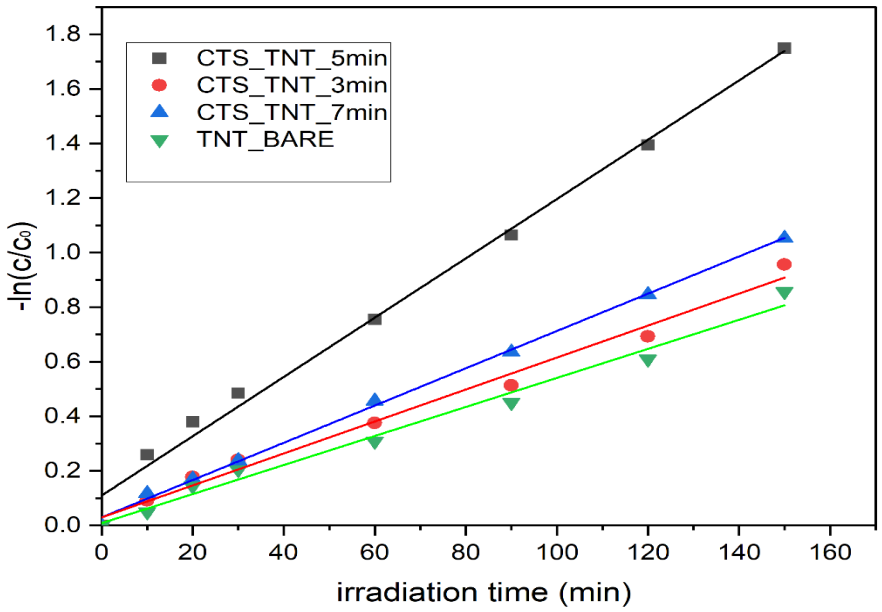

Figure 5.12. RhB degradation reaction kinetics fit under visible light.

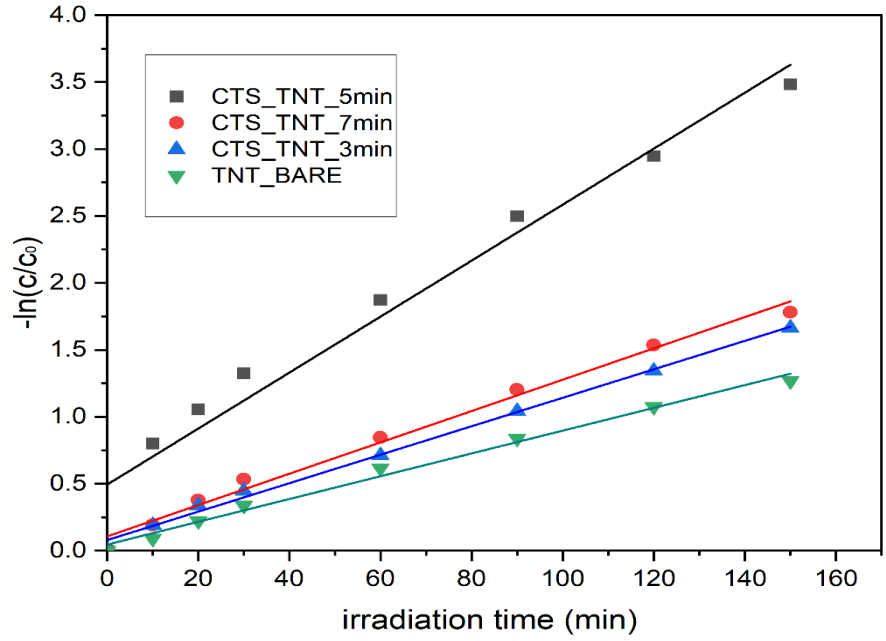

Figure 5. 13. RhB degradation reaction kinetics fit under UV light.

6. CONCLUSION

In this present research Cu_2SnS_3/TiO_2 nanotubes nanocomposite films have been synthesized in two steps ; anodic oxidation followed by spray pyrolysis methods to enhance the photo catalytic activity. The CTS was decorated on the TNT arrays by spray pyrolysis and it was characterized by FESEM and XRD techniques. The coating duration was 3, 5 and 7 minutes respectively, also the precursor concentration of CTS was steady along all the samples. The CTS_TNT films demonstrated an enhancement in photocatalytic activity for the photodegradation of Rhodamine B under UV irradiation and visible light. After Cu_2SnS_3 decoration the efficiency for degradation of Rhodamine B increased as compared to the bare TNT. After going through four cycles of degradation for RhB, CTS TNT films have shown high photostability. Finally, the percentage photodegradations of RhB on TNT bare was 65% and the best performance sample (CTS_TNT_5 min) was 98% under UV light. On the other hand, the photodegradation of RhB was tested by all samples under visible light, and the pest sample performance was (CTS_TNT_5 min) 80 %.

It was concluded that as-prepared CTS/TNT nanocomposite films, when processed using a straightforward two-step procedure, had the potential to develop into an efficient photocatalyst for the elimination of dyes and other associated harmful substances.

Also, it was concluded that, even though the performance under visible light was lower than under UV light, it was still good and could be used as a photocatalyst under visible light because UV light is harmful and high cost.

In this study, insights into the rational design of high-efficiency CTS_TNT nanocomposite photocatalysts were provided and an attempt was made to assist in the development of advanced photocatalyst models. According to the results obtained within the scope of the thesis, CTS_TNT nanocomposite structures have been developed as a partial solution to the fast charge recombination that limits the practical application of TiO_2. It is recommended that researchers develop these structures with monolithic three-dimensional (3D) materials and graphitic carbon nanomaterials.

REFERENCES

Abegunde, O. O., Akinlabi, E. T., Oladijo, O. P., Akinlabi, S., and Ude, A. U. (2019) "Overview of thin film deposition techniques", ***AIMS Materials Science***, 6(2), 174-199.

Akpan, U. G., and Hameed, B. H. (2009) "Parameters affecting the photocatalytic degradation of dyes using TiO_2-based photocatalysts", ***a review. Journal of hazardous materials***, 170(2-3), 520-529.

Alduran, Y. (2019) "The Effect of Metal Doping on TiO_2 for Photocatalytic Applications", Doctoral thesis, ***Izmir Institute of Technology***, izmir, 7-8.

Azushima, A., Kopp, R., Korhonen, A., Yang, D. Y., Micari, F., Lahoti, G. D., ... and Yanagida, A. (2008) "Severe plastic deformation (SPD) processes for metals" ***CIRP annals***, 57(2), 716-735.

Baylan, S. (2011) "Tin Kaplamaların Anodik Oksidasyonu", Yayımlanmış Yüsek Lisan Tezi, ***İstanbul Teknik Üniversitesi Fen Bilimleri Enstitüsü***, İstanbul, 75.

Beşli, N. "Bölüm 2: Yarı İletkenler", http://eng.harran.edu.tr/~nbesli/SEG/02.YariIletkenler.pdf, 12.02.2009.

Bhatkhande, D. S., Pangarkar, V. G., and Beenackers, A. A. C. M. (2002) "Photocatalytic degradation for environmental applications–a review. Journal of Chemical Technology & Biotechnology" ***International Research in Process, Environmental & Clean Technology***, 77(1), 102-116.

Bıyıklı, O. (2020) "Manufacturing and characterization of perovskite thin films using novel methods", Doctoral thesis. ***Izmir Institute of Technology***, izmir6-7,.

Borker, P., & Salker, A. V. (2006) "Photocatalytic degradation of textile azo dye over $Ce1- xSnxO_2$ series", ***Materials Science and Engineering: B***, 133(1-3), 55-60.

Caglar, B., Guner, E. K., Ersoy, S., Caglar, S., Özdemir, A. O., Özdokur, K. V., ... and Çırak, Ç. (2021) "Bi2S3 nanorods decorated on bentonite nanocomposite for

enhanced visible-light-driven photocatalytic performance towards degradation of organic dyes", ***Journal of Alloys and Compounds***, 885, 160964.

Çırak, B. B., Caglar, B., Kılınç, T., Karadeniz, S. M., Erdoğan, Y., Kılıç, S., ... and Çırak, Ç. (2019) "Synthesis and characterization of ZnO nanorice decorated TiO_2 nanotubes for enhanced photocatalytic activity", ***Materials Research Bulletin***, 109, 160-167.

Çırak, B. B.Davaslıoğlu, İ. Ç., Özdokur, K. V., Koçak, S., Çırak, Ç., Çağlar, B., and Ertaş, F. N. (2021) "WO_3 decorated TiO_2 nanotube array electrode: Preparation, characterization and superior photoelectrochemical performance for rhodamine B dye degradation", ***Journal of Molecular Structure***, 1241, 130673.

Çırak, Ç. (2016) "Güneş Pili Uygulamalarında Kullanılan Bazı Boyar Maddelerinin, TiO2 Nanotüpler Üzerine Adsorpsiyonun İncelenmesi", ***BAP FEN-A-220114-0064***, Erzincan, 4-6.

Demir, Z. (2018) "Farklı konsantrasyonlarda sentezlenen TiO_2/ZnO nanokompozit yapıların karakterizasyonu ve boya duyarlı güneş pili performanslarının incelenmesi", Master's thesis, ***Fen Bilimleri Enstitüsü***, Erzincan, 3-4

Eden, Ç. (2019) "Farklı sıcaklıklarda sentezlenen TiO_2/ZnO nanokompozit yapıların karakterizasyonu ve boya duyarlı güneş pili performanslarının incelenmesi", Master's thesis, ***Fen Bilimleri Enstitüsü***, Erzincan, 11-12

Fang, D., Luo, Z., Huang, K., & Lagoudas, D. C. (2011) "Effect of heat treatment on morphology, crystalline structure and photocatalysis properties of TiO_2 nanotubes on Ti substrate and freestanding membrane", ***Applied Surface Science***, 257(15), 6451-6461.

Ghori, M. (2018)" Synthesis and Functional Applications of Highly Photocatalytic TiO2 Based Surfaces: Al/TiO_2 and Au/TiO_2 Hybrid Structures" Doctoral thesis, ***der Technischen Fakultät der Christian-Albrechts-Universität zu Kie***, Germany, 3-4.

Greene, J. E. (2014) “Tracing the 5000-year recorded history of inorganic thin films from~ 3000 BC to the early 1900s AD”, ***Applied Physics Reviews***, 1(4), 041302.

Gupta, K. M., and Gupta, N. (2016) “Semiconductor materials: their properties, applications, and recent advances”, ***In Advanced Semiconducting Materials and Devices (pp. 3-40)***. Springer, Cham.

Habulin, M. and Knez, Z. (2001) “Activity and stability of lipases from different sources in supercritical carbon dioxide and near- critical propane”, ***Journal of Chemical Technology and Biotechnology***, 76(2), 1260-1266.

Hall, S. R., Szymanski, J. T., and Stewart, J. M. (1978) “Kesterite, Cu< 2)(Zn, Fe) SnS< 4), and stannite, Cu< 2)(Fe, Zn) SnS< 4), structurally similar but distinct minerals”, ***The Canadian Mineralogist***, 16(2), 131-137.

Hearne, G. R., Zhao, J., Dawe, A. M., Pischedda, V., Maaza, M., Nieuwoudt, M. K., ... and Witcomb, M. J. (2004) “Effect of grain size on structural transitions in anatase TiO_2: A Raman spectroscopy study at high pressure” ***Physical Review B***, 70(13), 134102.

Iijima, S. (1991) “Helical microtubules of graphitic carbon”, ***nature***, 354(6348), 56-58.

Indira, K., Mudali, U. K., Nishimura, T., & Rajendran, N. (2015) “A review on TiO_2 nanotubes: influence of anodization parameters, formation mechanism, properties, corrosion behavior, and biomedical applications”, ***Journal of bio- and tribo-corrosion***, 1(4), 1-22.

Karthikeyan, C., Arunachalam, P., Ramachandran, K., Al-Mayouf, A. M., & Karuppuchamy, S. (2020) “Recent advances in semiconductor metal oxides with enhanced methods for solar photocatalytic applications”, ***Journal of Alloys and Compounds***, 828, 154281.

Kelly, J. J. (1979) “The influence of fluoride ions on the passive dissolution of titanium”, ***Electrochimica Acta***, 24(12), 1273-1282.

Khan, M. M., Adil, S. F., and Al-Mayouf, A. (2015) “Metal oxides as photocatalysts”, ***Journal of Saudi Chemical Society***, 19(5), 462-464.

Kudret, A. (2011) "ZnO Tabanlı Doğal Boyar Maddeli Güneş Pili Yapımı", Yayımlanmış Yüksek Lisans Tezi, ***Kahramanmaraş Sütçü İmam Fen Bilimleri Enstitüsü***, Kahramanmaraş, 85.

Kustiningsih, I., Saripudin, C., Suwansih, S., and Sari, D. K. (2020) :Photocatalytic Degradation of Organic Waste in Visible light using TiO_2 Nanotubes Array", ***In IOP Conference Series: Materials Science and Engineering*** (Vol. 796, No. 1, p. 012060). IOP Publishing.

Lee, W. (2010) "The anodization of aluminum for nanotechnology applications", ***Jom***, 62(6), 57-63.

Lee, W. H., Lai, C. W., and Hamid, S. B. A. (2015) "One-step formation of WO_3-loaded TiO_2 nanotubes composite film for high photocatalytic performance", ***Materials***, 8(5), 2139-2153.

Li, X. Z., Li, F. B., Yang, C. L., and Ge, W. K. (2001) "Photocatalytic activity of WOx-TiO_2 under visible light irradiation", ***Journal of Photochemistry and Photobiology A: Chemistry***, 141(2-3), 209-217.

Lokhande, A. C., Chalapathy, R. B. V., He, M., Jo, E., Gang, M., Pawar, S. A., ... and Kim, J. H. (2016) "Development of Cu_2SnS_3 (CTS) thin film solar cells by physical techniques" ***A status review. Solar Energy Materials and Solar Cells***, 153, 84-107.

Mattox, D. M. (2010) Handbook of physical vapor deposition (PVD) processing 2nd ed., ***William Andrew***, Burlington 3-4

Nakashima, M., Yamaguchi, T., Itani, H., Sasano, J., and Izaki, M. (2015) "Cu_2SnS_3 thin film solar cells prepared by thermal crystallization of evaporated Cu/Sn precursors in sulfur and tin atmosphere" ***physica status solidi (c),*** 12(6), 761-764.

Onay, A. (2021) "Production of ce and cu doped nano-TiO_2 by flame spray pyrolysis method and evaluation of their photo-catalytic activities", Master thesis, ***the graduate school of natural and applied sciences of atilim university***, Ankara, 1-9.

Oba, F., and Kumagai, Y. (2018) “Design and exploration of semiconductors from first principles: A review of recent advances”; ***Applied Physics Express***, 11(6), 060101.

Onoda, M., Chen, X. A., Sato, A., and Wada, H. (2000) “Crystal structure and twinning of monoclinic Cu2SnS3” ***Materials Research Bulletin***, 35(9), 1563-1570.

Pal, B., Hata, T., Goto, K., and Nogami, G. (2001) “Photocatalytic degradation of o-cresol sensitized by iron–titania binary photocatalysts”, ***Journal of Molecular Catalysis A: Chemical***, 169(1-2), 147-155.

Pelaez, M., Nolan, N. T., Pillai, S. C., Seery, M. K., Falaras, P., Kontos, A. G., ... and Dionysiou, D. D. (2012) “A review on the visible light active titanium dioxide photocatalysts for environmental applications”, ***Applied Catalysis B: Environmental***, 125, 331-349.

Perednis, D., and Gauckler, L. J. (2005) “Thin film deposition using spray pyrolysis”, ***Journal of electroceramics***, 14(2), 103-111.

Prakash, J., Sun, S., Swart, H. C., and Gupta, R. K. (2018) “Noble metals-TiO_2 nanocomposites: from fundamental mechanisms to photocatalysis, surface enhanced Raman scattering and antibacterial applications”, ***Applied Materials Today***, 11, 82-135.

Qiu, B., Zhou, Y., Ma, Y., Yang, X., Sheng, W., Xing, M., and Zhang, J. (2015) “Facile synthesis of the Ti3+ self-doped TiO_2-graphene nanosheet composites with enhanced photocatalysis”, ***Scientific reports***, 5(1), 1-6.

Rahaman, S., Singha, M. K., Sunil, M. A., and Ghosh, K. (2020) “Effect of copper concentration on CTS thin films for solar cell absorber layer and photocatalysis applications”, ***Superlattices and Microstructures***, 145, 106589.

Rasoulifard, M., Fazli, M., and Eskandarian, M. (2014) “Kinetic study for photocatalytic degradation of Direct Red 23 in UV–LED/nano-TiO_2/S_2O_{82}− process: dependence of degradation kinetic on operational parameters”, ***Journal of Industrial and Engineering Chemistry***, 20(5), 3695-3702.

Rawya Abdul Ghani and Abdul Rahim, Tamadur Al-Mardi Al-Bashir. (2016) "Study of the optical properties of thin films", Doctoral thesis, ***Sudan University of Science and Technology***, Sudan.

Reddy, V. R. M., Pallavolu, M. R., Guddeti, P. R., Gedi, S., Reddy, K. K. Y. B., Pejjai, B., ... and Park, C. (2019) "Review on Cu_2SnS_3, Cu_3SnS_4, and Cu_4SnS_4 thin films and their photovoltaic performance", ***Journal of Industrial and Engineering Chemistry***, 76, 39-74.

Rossnagel, S. M. (2003) "Thin film deposition with physical vapor deposition and related technologies", ***Journal of Vacuum Science & Technology A: Vacuum, Surfaces, and Films***, 21(5), S74-S87.

Roy, P., Berger, S., and Schmuki, P. (2011) "TiO_2 nanotubes: synthesis and applications", ***Angewandte Chemie International Edition***, 50(13), 2904-2939.

Schneider, J., Matsuoka, M., Takeuchi, M., Zhang, J., Horiuchi, Y., Anpo, M., and Bahnemann, D. W. (2014) "Understanding TiO_2 photocatalysis: mechanisms and materials", ***Chemical reviews***, 114(19), 9919-9986.

Singh, P., Vishnu, M. C., Sharma, K. K., Borthakur, A., Srivastava, P., Pal, D. B., ... and Mishra, P. K. (2016) "Photocatalytic degradation of Acid Red dye stuff in the presence of activated carbon-TiO_2 composite and its kinetic enumeration", ***Journal of Water Process Engineering***, 12, 20-31.

Song, K. Y., Park, M. K., Kwon, Y. T., Lee, H. W., Chung, W. J., and Lee, W. I. (2001) "Preparation of transparent particulate MoO_3/TiO_2 and WO_3/TiO_2 films and their photocatalytic properties", ***Chemistry of Materials***, 13(7), 2349-2355.

Sönmezoğlu, S., Mehmed, K. O. Ç., ve Seçkin, A. K. I. N. (2012) "İnce film üretim teknikleri", ***Erciyes Üniversitesi Fen Bilimleri Enstitüsü Fen Bilimleri Dergisi***, 28(5), 389-404.

Stoian, M., Maurer, T., Lamri, S., and Fechete, I. (2021) "Techniques of Preparation of Thin Films: Catalytic Combustion", ***Catalysts***, 11(12), 1530.

Su, J., Zhu, L., and Chen, G. (2016) "Ultrasmall graphitic carbon nitride quantum dots decorated self-organized TiO2 nanotube arrays with highly efficient

photoelectrochemical activity" Applied Catalysis B: Environmental, 186, 127-135.

Su, J., Zhu, L., Geng, P., and Chen, G. (2016) "Self-assembly graphitic carbon nitride quantum dots anchored on TiO_2 nanotube arrays: An efficient heterojunction for pollutants degradation under solar light", ***Journal of hazardous materials***, 316, 159-168.

Thirumalai, J. (2017) "Introductory Chapter: The Prominence of Thin Film Science in Technological Scale", ***Thin Film Processes-Artifacts on Surface Phenomena and Technological Facets***.

Van Viet, P., Trang, D. D. P., Dai Phat, B., and Thi, C. M. (2018) "Understanding the effect of annealing temperature on crystalline structure, morphology, and photocatalytic activity of silver-loaded TiO_2 nanotubes", ***Superlattices and Microstructures***, 117, 305-316.

Vinodgopal, K., and Kamat, P. V. (1995) "Enhanced rates of photocatalytic degradation of an azo dye using SnO_2/TiO_2 coupled semiconductor thin films", ***Environmental science & technology***, 29(3), 841-845.

Vogel, R., Hoyer, P., and Weller, H. (2002) "Quantum-sized PbS, CdS, Ag_2S, Sb_2S_3, and Bi_2S_3 particles as sensitizers for various nanoporous wide-bandgap semiconductors", ***The Journal of Physical Chemistry***, 98(12), 3183-3188.

Wang, B., Huang, W., Chi, L., Al-Hashimi, M., Marks, T. J., and Facchetti, A. (2018) "High-k gate dielectrics for emerging flexible and stretchable electronics", ***Chemical reviews***, 118(11), 5690-5754.

Wang, N. (1974) "The three ternary phases in the system cu-sn-s", ***Neu. jb. mineral., monatsh.; dtsch***, P. 424 A 431

Yao, S., Xu, L., Gao, Q., Wang, X., Kong, N., Li, W., ... and Pu, X. (2017) "Enhanced photocatalytic degradation of Rhodamine B by reduced graphene oxides wrapped-Cu_2SnS_3 flower-like architectures", ***Journal of Alloys and Compounds***, 704, 469-477.

Yüksel, A. (2021) “Tavlama sicakliğinin anodik oksidasyon ile büyütülen TiO_2 nanotüplerin fotokatalitik aktivitelerine etkisi”, Master thesis, ***Fen Bilimleri Enstitüsü, Erzincan***, 51-52.

Yu, J. C., Lin, J., and Kwok, R. W. (1998) “Ti1-x Zr x O_2 Solid Solutions for the Photocatalytic Degradation of Acetone in Air”, ***The Journal of Physical Chemistry B***, 102(26), 5094-5098.

Zhou, X., Liu, N., and Schmuki, P. (2017) “Photocatalysis with TiO_2 nanotubes:“colorful” reactivity and designing site-specific photocatalytic centers into TiO2 nanotubes”, ***ACS Catalysis***, 7(5), 3210-3235.

Zwilling, V., Darque-Ceretti, E., Boutry-Forveille, A., David, D., Perrin, M. Y., and Aucouturier, M. (1999) “Structure and physicochemistry of anodic oxide films on titanium and TA6V alloy”, ***Surface and interface analysis***, 27(7), 629-637.